Recent developments and future perspectives of reverse electrodialysis technology: A review

Ying Mei[1], Chuyang Y. Tang [1, *]

[1] Department of Civil Engineering, The University of Hong Kong, Pokfulam Road, Hong Kong S.A.R., P.R. China

*Corresponding author address: HW6-19B Haking Wong Building, Department of Civil Engineering, the University of Hong Kong, Pokfulam, Hong Kong; Tel: (+852) 28591976; E-mail: tangc@hku.hk

Abstract

Reverse electrodialysis (RED) is an emerging membrane based technology that captures electricity from controlled mixing of two water streams of different salinities. To date, great advancements have been achieved on the development of RED components (e.g., membranes and spacers), optimization of operational conditions, and development of hybrid processes. This review presents an overview on the current achievements in RED membranes and spacers. Meanwhile, the critical operation conditions and their interconnected relationships are highlighted. Moreover, several innovative hybrid systems that show strong synergistic effects are highlighted. The latest development of nano-/micro-fluidic RED and pilot scale tests are also summarized.

Keywords: Salinity gradient power (SGP); Reverse electrodialysis (RED); Ion exchange membranes; Hybrid membrane process; Desalination

Contents

1. Introduction

Salinity gradient power (SGP) can be harvested from mixing water streams of different salinity. Theoretically, approximately 0.8 kWh is obtainable when 1 m^3 of fresh water flow into the sea, which translates into nearly 2 TW of SGP on the basis of the total freshwater flow of the major rivers worldwide (Fig. 1) [1]. The global hydrological cycle makes SGP a renewable energy. Other feed streams, such as treated waste water effluents and desalination brine can further extend the scope of SGP [2-4]. Synthetic high-salinity draw solutions (e.g., ammonium bicarbonate or sodium chloride) have also been investigated for recovering low grade waste heat in a closed-loop osmotic heat engine [5-7] and for energy storage as a concentration battery [8, 9].

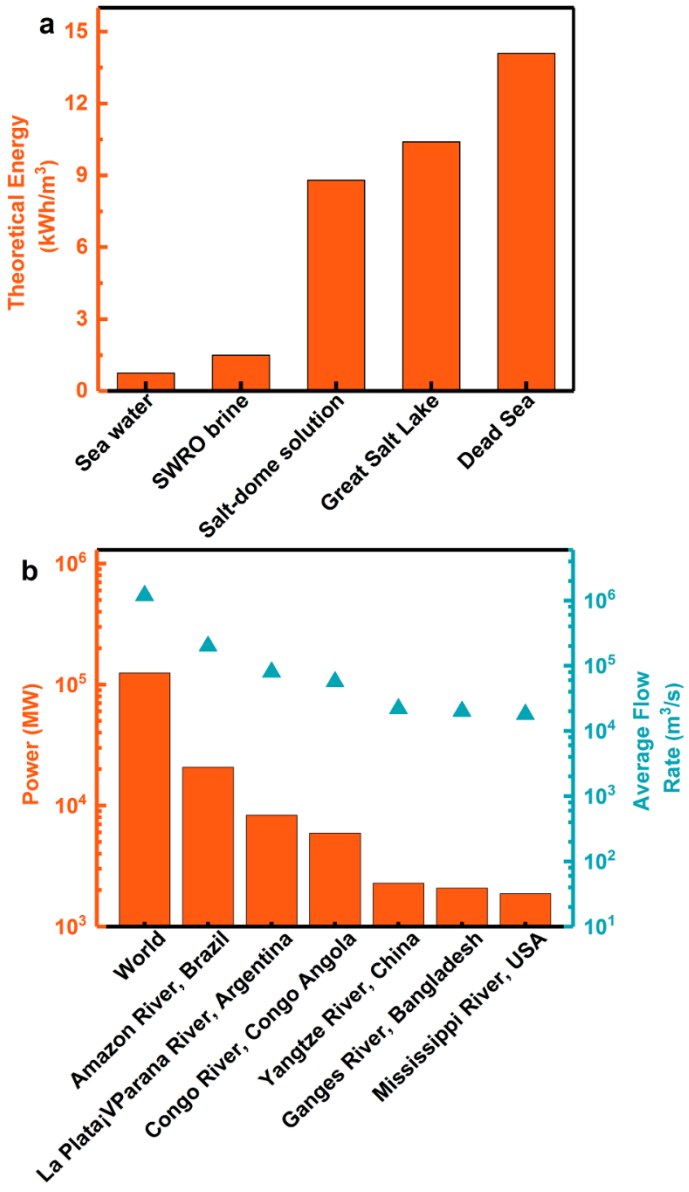

Fig. 1. (a) Maximum extractable energy from mixing fresh water with saline water using different high-salinity sources; (b) osmotic power production capacity from selected major rivers across the world. Figure adapted from reference [10] with copyright permission from Elsevier.

Reverse electrodialysis (RED) is a mainstream technology for harvesting SGP [11, 12]. A typical RED stack comprises of cation exchange membranes (CEMs) and anion exchange membranes (AEMs) assembled in an alternating order to form flow compartments of high salinity streams (HS) and low salinity streams (LS) (Fig. 2). Cations and anions in the HS transport to LS through CEM and AEM in opposite directions under their respective

concentration gradients, which can be converted to electricity by redox reaction on the electrodes.

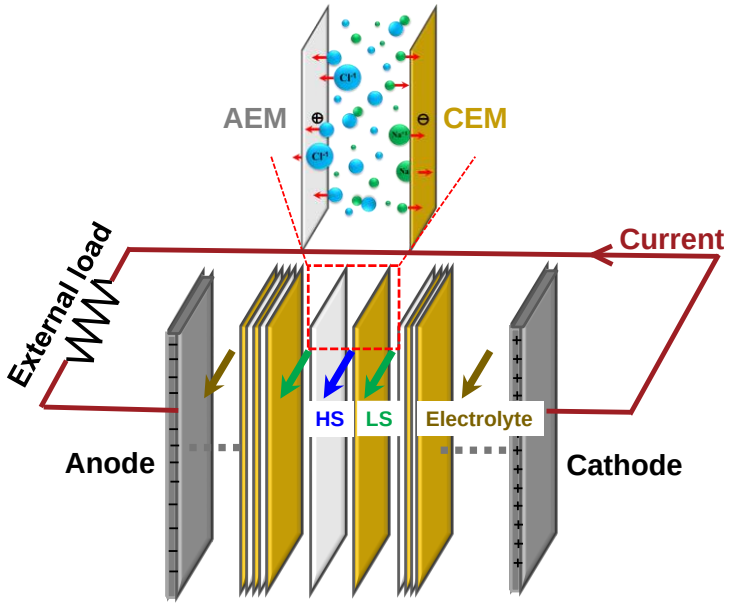

Fig. 2. Schematic diagram of an RED stack connected to an external electric load.

Several review papers on RED are already available in the literature. Progresses up early 2011 have been summarized by Post et al. [12] and Ramon et al. [13]. In a perspective paper published in 2012, Logan and Elimelech [1] provided an overview of different SGP harvesting technologies (e.g., RED, pressure retarded osmosis). Detailed comparisons of these methods were performed by Yip et al. [11, 14]. Logan and Elimelech [1] also highlighted the critical challenge of IEMs development for RED. Readers who are interested in the development of IEMs are further referred to Hong et al. [15, 16] and Xu [17].

Despite these existing reviews, there is still lack of a comprehensive summary on the latest developments in RED, particularly in view of the exponentially increasing number of publications in the last decade (Fig. 3). These studies can be classified on the basis of their primary focus on RED module optimization [18-23] (including IEMs, spacers and electrodes),

stack operation [24-27] (e.g., temperature, feed solution concentrations, flow path, etc.), hybrid process development [5, 28-34] (e.g., microbial reverse electrodialysis cells, hybrid RED/reverse osmosis system, RED using thermolytic solutions, etc.) and nano-/micro-fluidic RED development [35, 36]. Over the past five years, the RED research scope has been rapidly expanded, and systematic efforts on fouling investigation [37-39], applications for energy storage and pollutants abatement [8, 9, 40, 41] and pilot studies [3, 42] have been reported. A comprehensive review is thus warranted to address these recent developments in RED technology.

This review starts with an overview of historical developments in RED, followed by an introduction of basic theory of RED. Subsequently, recent progresses in IEMs and other module components (i.e., spacers and electrodes) and studies on optimization of operational conditions are summarized. Meanwhile, hybrid RED systems (e.g., by combining RED with microbial fuel cell or electrodialysis) as well as some special RED applications (e.g., energy storage, pollutants abatement, and nanofluidic/microfluidic RED devices) are highlighted. Practical considerations such as membrane fouling and pilot testing are also discussed.

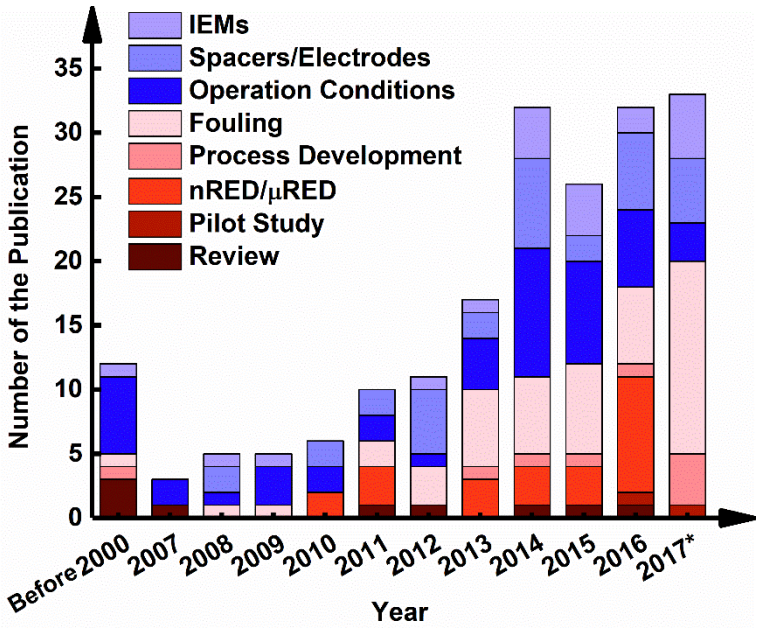

Fig. 3. Number of publication on RED since 1954. Publications are categorized based on their main research focus. The data are obtained from Scopus and Google Scholar databases by September 2017. Keyword for searching is 'reverse electrodialysis'.

2. Historical development of RED

2.1. Early studies before 2000s

Fig. 4 presents a summary of the historical development of RED technology. In 1954, Pattle [43] first described the concept of salinity gradient power. Using a bench scale 'hydroelectric pile' comprised of 47 pairs of alternating acidic and basic membranes of 8 cm^2 each, he obtained a power output of 0.2 W/m^2 and an electromotive force of 3.1 V from mixing fresh and seawater at 39 °C. Not until two decades later, theoretical models of RED were developed by Fair and Osterle in 1971 for RED in charged capillary membranes [44] and by Weinstein and Leitz [25] in 1976 for IEM stacks. Early theoretical studies revealed that the power production by RED can be potentially competitive against other alternative energy sources [45, 46]. However, early experimental works often show impractically low power density (e.g., merely 0.4 W/m^2 using a hypersaline NaCl solution of 250 g/L paired to a 1 g/L NaCl [47]) and low energy conversion efficiency (e.g., 1.8 % - 11.7 % [48]). During this early phase of

development, we also witness the first report on RED fouling by Ratkje et al. in 1986 [49] and the first hybrid RED/electrolysis system (which was used for simultaneous electricity generation by RED and acid and base production in the electrode compartments [50]).

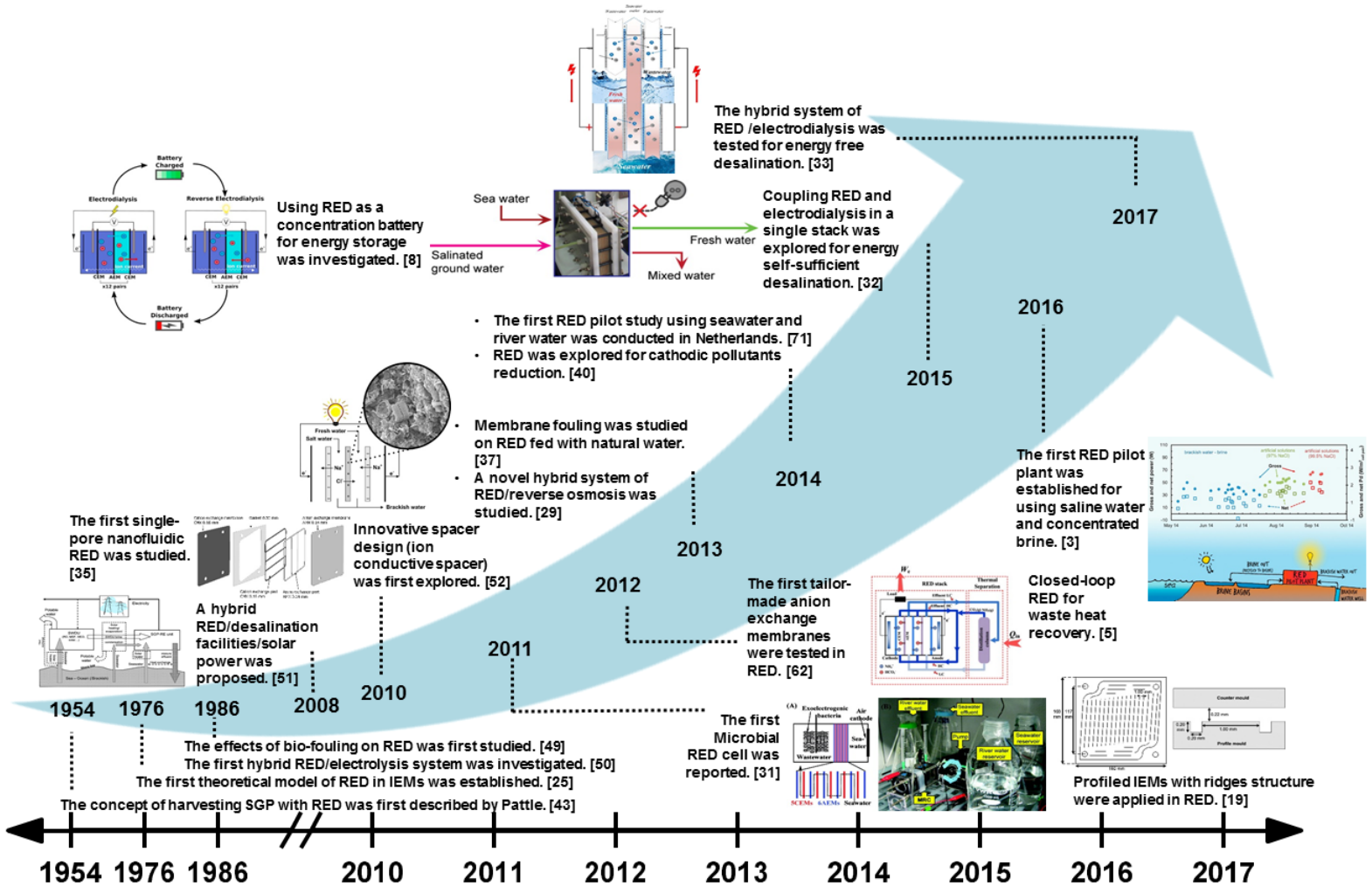

Fig. 4. Historical development of RED technology (some parts of the figure are taken from [3, 5, 8, 19, 31-33, 37, 51, 52] with copyrights permission from Elsevier and ACS Publications.)

2.2. Studies during early 2000s

Extensive researches on RED emerged in early 2000s (Fig. 4), which coincides with the spike in the cost of fossil fuel energy [53]. During this period, systematic studies on the role of IEMs [54, 55], stack configuration [18, 54, 56, 57] and operation conditions [57-61] in RED power generation were performed. With the availability of commercial IEMs and improved stack design, significant improvement in power density was realized (e.g., a maximum value of 0.93 W/m^2 was obtained using NaCl of 0.5 M and 0.017 M as feed solutions [55, 60]). Meanwhile, hybrid processes of RED/desalination facilities/solar power were proposed by Brauns to realize simultaneous energy production and water purification [51, 59].

2.3. Studies in 2010s

Tremendous advances in RED performance have been achieved over last decade with the exciting progresses in IEMs and spacer designs. In 2012, the first tailor-made IEM specifically designed for RED showed a power density of 1.27 W/m^2 [62]. This has been followed by a wave of RED membrane development work [21, 63-66]. The majority of these tailor-made RED membranes are homogeneous; most of them have much thinner membrane thickness (26 – 91 μm) compared to conventional IEMs used for electrodialysis in order to achieve lower electric resistance (0.28 – 2.26 $\Omega \cdot cm^2$). Nano/microfluidic RED using ion-selective nanochannels show further dramatic increase in power density (e.g., a power density of 20-2600 W/m^2 was expected for a porous membrane) [35, 36]. Meanwhile, innovative spacer designs (e.g., tailor-made IEMs with ridges/pillar structures [19, 67], ion conductive spacers [52], and the use of ion exchange resin as space separators [68]) lead to enhanced power density by up to 4 times. With the improvements of RED power generation, considerable efforts have concentrated on innovative applications of RED, e.g., osmotic heat engine for converting low grade heat to electricity [5], concentration battery for energy storage [8, 9, 69], microbial RED

cell for synergistic energy harvesting [30, 31], and for RED based recalcitrant pollutants abatement [40, 41, 70]. During the last decades, we have also witnessed the commissioning of RED pilot plants in the Netherlands [71] and Italy [3, 42], which is a critical step to its practical implementation at large scales. These pilot tests have been supplemented by lab-scale fouling investigations [37, 38, 72]. However, there is yet no full scale RED plants up to day.

3. Basic theory of RED

3.1 Electrochemical membrane processes

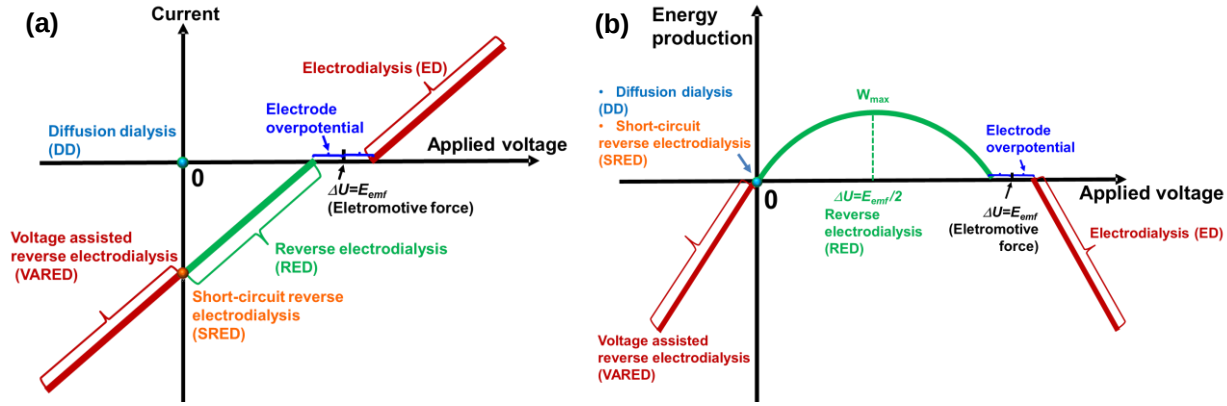

Fig. 5. (a) Current as a function of applied voltage in ED, RED, SRED, VARED, and DD; (b) energy output as a function of applied voltage in in ED, RED, SRED, VARED, and DD. ED process where electrical energy is consumed to drive ionic transport against the concentration gradient; RED process where electricity is generated from ionic current along the concentration gradient; VARED process where electricity is consumed to further enhance the ionic transport from the concentrated solution to dilute solution; SRED and DD processes where electricity is neither consumed nor generated.

Fig. 5 provides a useful overview of the relationship between electrodialysis (ED), RED, short-circuit reverse electrodialysis (SRED), voltage assisted reverse electrodialysis (VARED), and diffusion dialysis (DD). ED is a well-established desalination method, where an external electrical voltage is applied to overcome the electromotive force (in addition to any overpotential at the electrodes) such that ions migrate against their respective concentration

gradient to obtain desalted water [73, 74]. In contrast, the electrical voltage in RED is lower than the electromotive force such that ions move under the concentration gradient to generate an ionic current that has opposite direction to the electrical field. Whereas ED consumes electricity, its reverse process RED produces electricity from salinity gradient; their power density is given by the product of the electrical voltage output and the corresponding current density. Under the special condition where the electrical voltage output is 0 (close-circuit condition), electricity is neither produced nor consumed. In this case, ions can diffuse under their respective concentration gradients at rates faster than the corresponding ones under RED conditions; this process is referred as SRED in this paper. To further enhance the rates of transport of ions, an external voltage can be applied in the same direction to the ionic current. This configuration, referred as VARED, accelerates the ion removal from the high concentration stream at the expense of additional energy consumption compared to SRED. Both SRED and VARED can have potential applications in desalination by removing salts from the high concentration solution at accelerated rates. The electrochemical membrane processes ED, RED, SRED, and VARED are analogous to their pressure/osmotic-pressure-driven counterparts reverse osmosis, pressure retarded osmosis, forward osmosis, and pressure-assisted forward osmosis, respectively [75-79]. DD is a process similar to SRED in that no external voltage is applied. However, instead of using both AEMs and CEMs in an alternative sequence in SRED, only one type of membrane is used in DD. DD processes using AEMs are commonly applied for recovering acids [80-84]. In these applications, the transport of anions (e.g., Cl^-, SO_4^{2-} or NO_3^-) under their concentration gradient across an AEM is accompanied by H^+ as a counter-ion due to its small size and high mobility; electroneutrality is maintained during the transport of ions such as no net electric current is produced [85]. For this reason, DD is located at the origin of the plot in Fig. 5a,b. In a similar manner, DD processes using CEMs can be used for separating base containing solutions [85]. To further accelerate the ions

183 migration in DD, a voltage assisted diffusion dialysis (VADD) can be used by applying an
184 external electric field in the same direction as the concentration gradient [86].
185
186 ## 3.2 Analytical model of RED
187 The extractable SGP energy from mixing LS of volume V_{LS} and HS of volume V_{HS} at constant
188 pressure and temperature can be calculated as the Gibbs free energy of mixing ΔG_{mix} [18, 87,
189 88] (Fig. 6):
190 $$\Delta G_{mix} = RT\left\{\left[\sum_i c_i ln(\gamma_i \cdot c_i)\right]_{LS} + \frac{(1-f)}{f}\left[\sum_i c_i ln(\gamma_i \cdot c_i)\right]_{HS} - \frac{1}{f}\left[\sum_i c_i ln(\gamma_i \cdot c_i)\right]_{mix}\right\} \quad (1)$$
191 where R is the universal gas constant (8.314 J/mol· K), T is the absolute temperature, f is the
192 volume fraction of LS to the total feed solutions (i.e., $f = V_{LS}/V_{mix}$), c_i is the molar
193 concentration of component i in aqueous solutions (i = Na^+, Cl^-, H_2O, etc.), γ is the activity
194 coefficient, the subscripts *mix*, *HS* and *LS* indicated mixed effluent, HS and LS, respectively.
195

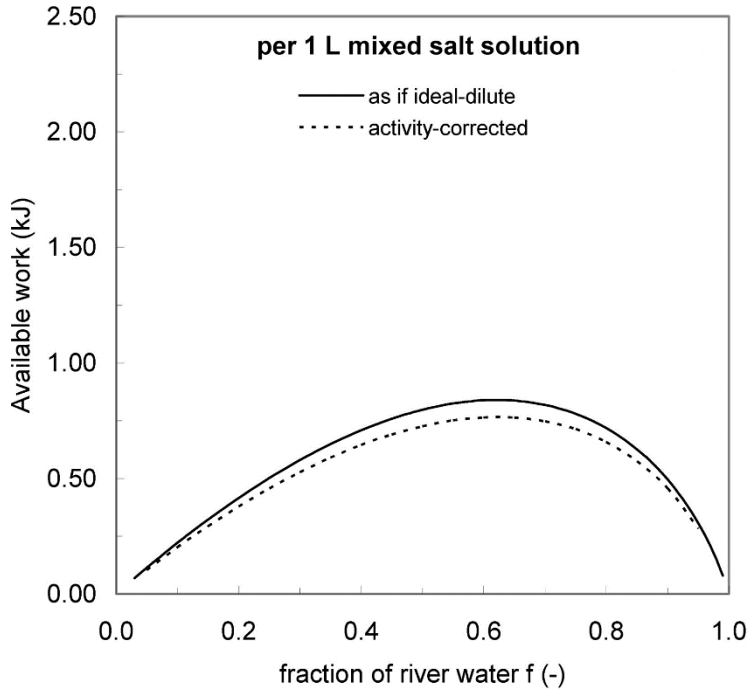

196
197 **Fig. 6. The Gibbs free energy released per liter of mixing solution, where *f* is the fraction of LS and (1-*f*) is the fraction**
198 **of HS at temperature of 293 K. Figure is obtained from [18] with copyright permission from ACS Publications.**

The theoretical electromotive force E_{emf} (V) can be calculated based on the Nernst equation [18, 57]:

$$E_{emf} = \frac{N_m \alpha RT}{zF} ln\left(\frac{\gamma_{HS} \cdot c_{HS}}{\gamma_{LS} \cdot c_{LS}}\right) \quad (2)$$

where N_m is the number of IEMs, α is the average membrane permselectivity, F is the Faraday constant (96485 C/mol), z is the ionic valence (1 for Na^+ and Cl^-) [54].

When RED is connected to an external load, the voltage output U (Fig. 7a) can be calculated as the difference between the electromotive force E_{emf} and the voltage drop across the internal resistance R_{stack} [88]:

$$U = E_{emf} - JAR_{stack} \quad (3)$$

where J (A/m^2) is current density in the electrical circuit, A (m^2) is projected area of IEMs. The above relationship between the voltage output and current density can be plotted as polarization curve (Fig. 7a), where its slope represents the area resistance of RED stack (AR_{stack}). R_{stack} is the sum of ohmic resistance of stack components and non-ohmic resistance (e.g., due to concentration polarization in water compartment) [13, 18, 89].

$$R_{stack} = R_{ohmic} + R_{nonohmic} \quad (4)$$

$$\text{with } R_{ohmic} = \frac{N_m}{A}\left[\bar{R}_{CEM} + \bar{R}_{AEM} + \frac{1}{\sigma}\left(\frac{d_{HS}}{c_{HS}} + \frac{d_{LS}}{c_{LS}}\right)\right] + R_{El} \quad (5)$$

where $\bar{R}_{CEM}$ and $\bar{R}_{AEM}$ are the area resistance of AEM and CEM ($\Omega \cdot cm^2$), respectively, and R_{El} is the area resistance of electrodes ($\Omega \cdot cm^2$). The term $\frac{1}{\sigma}\left(\frac{d_{HS}}{c_{HS}} + \frac{d_{LS}}{c_{LS}}\right)$ in Eq. (5) represents the area resistance of HS and LS compartments, in which σ is the molar conductivity of solution species ($s \cdot cm^2/mol$), d is the intermembrane distance (cm), and c is the molar concentration of electrolyte (mol/L).

Thus, the power generation P (W/m^2) can be expressed as (Fig. 7b) [89]:

$$P = J^2(R_L A) = \left(\frac{E_{emf}}{R_{stack}+R_L}\right)^2 \frac{R_L}{A} = U \cdot J \cdot A \quad (6)$$

where R_L is the external resistance (Ω). The maximum power density P_{max} can be obtained when the resistance of external load R_L equals the internal resistance of the RED stack R_{stack} [57]:

$$P_{max} = \frac{{E_{emf}}^2}{4 \cdot R_{stack}} \quad (7)$$

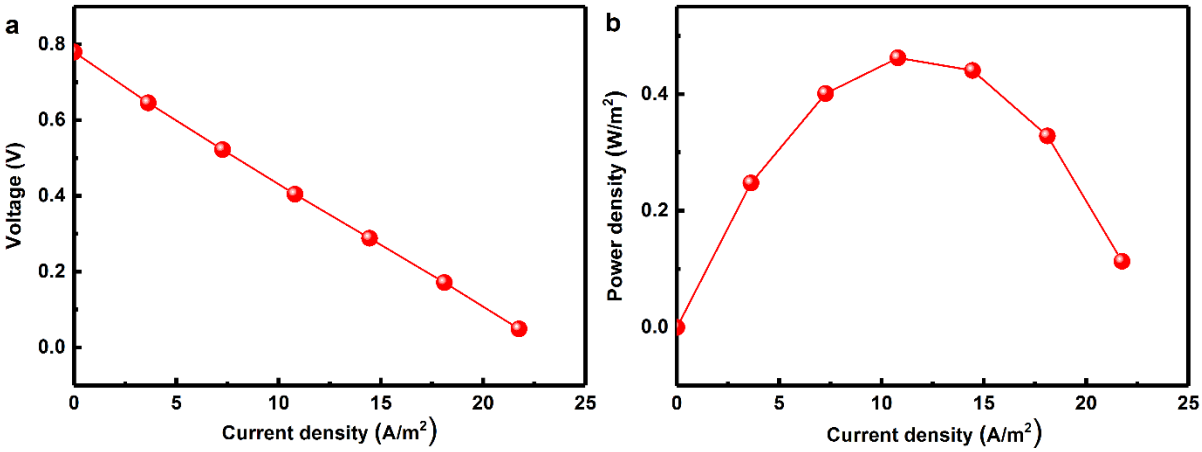

Fig. 7. (a) The voltage output and (b) power density of an RED stack vs. the current density. Experimental conditions: five pairs of CEMs and AEMs from Selemion®, spacers with thickness of 0.2 mm from Nitex®, HS of 0.6 M NaCl and LS of 0.02 M NaCl.

The energy efficiency η is determined by the captured electric energy compared to the theoretical amount of Gibbs free energy released during the mixing process [90]:

$$\eta = \frac{P \cdot A}{\Delta G_{mix} \cdot \phi} \quad (8)$$

where Φ is the volumetric flow rate of LS (m^3/s).

4. RED module components

4.1. IEMs

Substantial improvements on RED module components have been reported in recent years. The latest progresses in spacers and electrodes are highlighted in Sections 4.2 and 4.3, respectively. In the current section, we report the recent developments in RED membranes.

4.1.1. IEMs basics

The most common way to classify IEMs is based on their charged functional groups: CEMs contain negatively charged groups (e.g., sulfonic acid ($-SO_3^-$), carboxylic acid ($-COO^-$), phosphoryl ($-PO_3^{2-}$), and phosphonic acid ($-PO_3H^-$)) that selectively permit the passage of cations but reject anions; AEMs contain positively charged groups (e.g., ammonium ($-NH_3^+$), secondary amine ($-NRH_2^+$), tertiary amine ($-NR_2H^+$), quaternary amine ($-NR_3^+$)) that selectively transport anions but exclude cations [17]. Based on the manufacture method and its physical structure, an IEM can be either homogeneous or heterogeneous [91]. In a homogeneous membrane, the membrane matrix is uniformly charged (Fig. 8a). In contrast, a heterogeneous membrane (Fig. 8b), often containing uncharged binding polymer separates charged domains of ion exchange resin, is characterized with non-uniform charge distribution [17]. Homogeneous membranes can be further classified with respect to their preparation procedures into two main categories: (1) membranes prepared from copolymerization of monomers (e.g., styrene and divinylbenzene), which can be functionalized (e.g., chloromethylation-amination for CEMs and sulfonation for AEMs), (2) membranes made from polymer, either polymer film (e.g., hydrocarbon polyethylene (PE), polypropylene (PP), and fluorocarbon, etc.) or polymer solution (e.g., polystyrene (PS)), and followed by grafting functional monomers or non-functional monomers which can be further functionalized [17, 91, 92]. In contrast, heterogeneous membranes are commonly made from blending

powdered/melted ion exchange resin with uncharged polymer (e.g., polyvinylchloride (PVC), acrylonitrile, etc.) and pressing/casting into membrane films [92]. Furthermore, several new fabrication strategies have emerged in the literature, with great potential to improve IEMs properties [93]. Some notable examples include blending of two or more polymers (e.g., combination of fluorinated/non-fluorinated polymers) to achieve synergistic effects of each component [94], pore filling of porous substrate with polymer electrolyte to realize simultaneous high stability and selectivity [64, 66], in-situ polymerization using liquid monomer, and electro-spinning of nano-fiber IEMs.

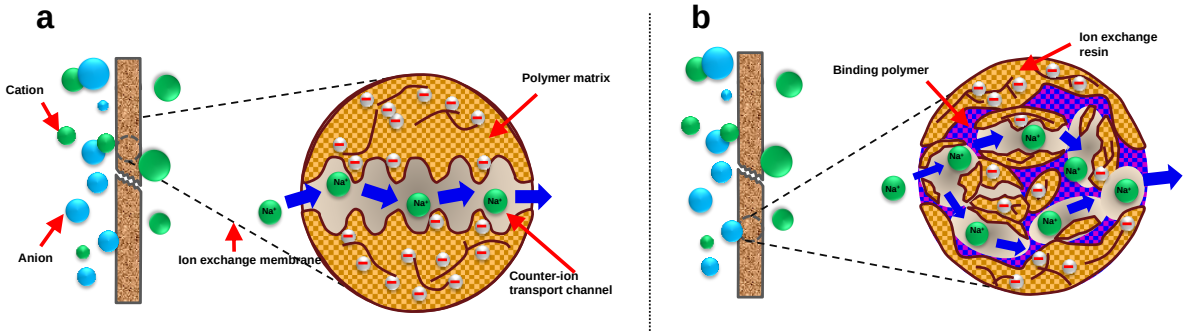

Fig. 8. Schematic diagrams of the internal structure of (a) a homogeneous membrane in which fixed charges uniformly distribute in the polymer matrix and (b) a heterogeneous membrane in which charged domains of ion exchange resin mix with uncharged binding polymer.

4.1.2. IEMs properties

The most important properties of IEMs include permselectivity and electrical resistance, which critically determines power output performance of RED. Other parameters, such as water content, ion exchange capacity (IEC) and fixed charge density (FCD) can affect RED performance through their influence on permselectivity and electrical resistance.

Water content is of crucial importance to membrane dimensional stability and ionic transport properties [95]. High water content implies a loose mechanical structure and often results in

poor permselectivity, despite its positive effect on membrane conductivity [15, 96]. It is influenced by membrane material, fixed charged groups, cross-linking degree of membrane matrix and surrounding solution conditions [92]. For example, some AEMs with relatively low cross-linking degrees tend to have higher water contents than their more crosslinked CEMs counterparts [54]. Water content of a specific membrane can be experimentally quantified by measuring membrane swelling degree (SD) [96]:

$$SD = \frac{m_{wet} - m_{dry}}{m_{dry}} \times 10 \quad (9)$$

where m_{wet} is weight of IEM in wet condition and m_{dry} is weight of membrane sample in its corresponding dry phase.

Ion exchange capacity (IEC) represents the number of fixed charged groups in the membrane matrix. It is determined as the milli-equivalents (meq) of charged groups per gram of dry membrane [54]. IEC is generally tested experimentally through determining the number of counter-ions (e.g., cations in the case of CEM and anions in the case of AEM) after turning CEMs into H^+-saturated form and AEMs into Cl^--saturated form [54]. Since the presence of large quantities of fixed charges promotes membrane swelling, high IEC is typically accompanied by a high SD [96, 97]. While high IEC tends to increase membrane permselectivity, a high SD may dilute the effectiveness of IEC and adversely affect the permselectivity [15, 96]. Such competing effects call for a compromise between of IEC and SD. Another useful concept is fixed charge density (FCD), which is defined as the milli-equivalents of charged groups per gram of water in the membrane (meq/g H_2O) [96]. FCD can be used to better correlate with membrane permselectivity and resistance, and its value can be determined as the ratio of IEC over SD.

$$FCD = \frac{IEC}{SD} \quad (10)$$

Permselectivity indicates the ability of IEMs to selectively transport counter-ions (e.g., cations in the case of CEM) and exclude co-ions (e.g., anions in the case of CEM) [54]. Ideally, a perfect IEM shall have a permselectivity of 1 so that co-ions are completely prevented from migrating through membrane matrix. In practice, co-ions transport is inevitable, resulting in membrane permselectivity of less than 1. A higher permselectivity increases the voltage output according to equation (2). Permselectivity is usually calculated as the ratio of measured electrical potential difference across a membrane sample under a given concentration gradient and the corresponding theoretical value with an ideal membrane based on equation (2). A typical testing cell for permselectivity measurement is showing in Fig. 9 [15, 54, 95].

$$\text{Permselectivity} = \frac{E_{meas}}{E_{theo}} \times 100\% \quad (11)$$

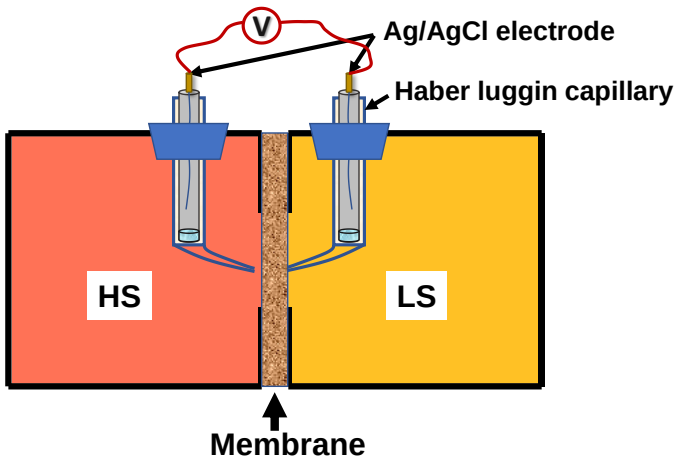

Fig. 9. Schematic diagram of an experimental setup with two compartments for characterizing membrane permselectivity under a given concentration gradient of HS and LS.

According to Donnan theory, increased FCD leads to enhanced electrostatic exclusion of co-ions, thus higher membrane permselectivity is achievable [54, 62, 98]. For example, some more cross-linked CEMs of high FCD usually shows higher permselectivity than their corresponding

AEMs (Table 1) [54, 96]. However, the effectiveness of electrostatic exclusion may also be influenced by surrounding solution concentrations (e.g., high salt solution concentration adversely affects electrostatic exclusion) [95]. For instance, membrane permselectivity generally decreases as salt solution concentration increases. It is attributed to the interactive effects of increased FCD (i.e., water content decreases due to osmosis deswelling) and weakened electrostatic exclusion in concentrated solution. These observations suggest that membrane permselectivity shall be influenced by both membrane properties (e.g., IEC, SD, and FCD) and surrounding circumstances which would impact membrane properties in return.

Membrane resistance describes the hindrance of polymer matrix to ionic current transportation. It represents a major contribution to the internal resistance of an RED stack, and higher membrane resistance increases the voltage drop over the RED stack and thus reduces available power output [54]. Ionic transport through membrane matrix is realized by ions in the mobile phase, including counter-ions compensate to fixed charges at the internal surface of membrane pores and additive counter-ions pair with co-ions in the aqueous phase within membrane matrix [99]. The concentration and mobility of ion tend to be highly sensitive with water content of membrane polymer [100, 101], as well as the concentration of external salt solution concentration [99]. In addition, higher temperature can increase ion mobility substantially [54]. Therefore, lower membrane resistance is expected for IEMs with higher IEC, lower cross-linking degree, higher salt solution concentration and elevated temperature [102]. For example, IEMs of high IEC accompanied with high SD (commonly demonstrate a low FCD) usually have a relatively low area resistance and poor permselectivity [103]. Further increasing the cross-linking degree of membrane matrix (leads to higher FCD) would result in higher membrane resistance and better permselectivity (e.g., CEMs tends to have high FCD and high resistance than its corresponding AEMs), despite its positive effects on membrane mechanical

strength. It should be noted that there is no straight forward relationship between FCD and membrane resistance, which might also be influenced by membrane types and chemistry [96]. Especially, some heterogeneous membranes have relative low FCD than homogeneous membranes illustrated considerable high resistance due to the uncharged interstices, separation charged structures [104].

Membrane resistance can be measured in salt solutions by either direct current (DC) or alternative current (AC) method. Chronopotentiometry is a widely-used DC characterization method for membrane resistance, the result of which also includes ionic transport resistance in aqueous layers adjacent to the membrane surface (i.e., diffusion boundary layer (DBL) and electrical double layer) [57, 105]. During measurement, the voltage drops across a membrane under concern is recorded under a series of current density. The membrane area resistance is calculated as the slope of voltage output vs. current density curve. In addition, electrochemical impedance spectroscopy (EIS) using AC can also be applied to differentiate pure membrane resistance from the resistance emerged in the adjacent aqueous layer [106].

As stated above, membrane permselectivity and resistance are both influenced by interactive effects of IEC and SD. A membrane of low area resistance by low selectivity and vice versa [54]. There often needs a compromise between permselectivity and resistance in order to achieve optimized power performance of RED system based on the specific application goal. For example, a RED stack for harvesting SGP might favor IEMs of low area resistance in the sacrifice of moderate permselectivity, due to the critical role of internal resistance in power generation [54].

4.1.3. Tailor-made IEMs for RED

Table 1 summarizes the properties of IEMs that have been used for RED testing. Although most of reported studies on RED used commercially available IEMs (which are traditionally used for ED applications), there have been increasing number of publications on custom-made IEMs that are specially tailored for RED. Depending on the main focuses of these studies, they can be classified into three categories: (1) new ion exchange membrane materials, (2) innovative membrane manufacturing methods, and (3) novel membrane geometries. In 2012, Guler et al. reported the first AEM designed for RED, which was fabricated from polyepichlorohydrin (PECH) and introduced with anionic group using 1,4-diazabicyclo-[2.2.2.]octane (DABCO) [62]. This approach avoided the use of toxic chloromethylation chemicals. By using a thin membrane thickness of 33 μm, the resulting AEM had a relatively low area resistance (0.82 Ωcm^2), corresponding to a power density of 1.27 W/m^2 using 0.507 M and 0.017 M NaCl synthetic feed solutions. These authors further developed tailor-made CEMs that were fabricated from sulfonated polyetheretherketone (SPEEK) [96]. Chen and co-workers performed systematic investigations on tailored organic–inorganic nanocomposite CEMs [63, 107, 108] as well as organic-organic hybrid CEMs [94]. Introducing inorganic nanomaterials (e.g., sulfonated iron (III) oxides (Fe_2O_3-SO_4^{2-}), sulfonated silica (SiO_2-SO_3H) and oxidized multi-walled carbon nanotubes (O-MWCNTs)) into an organic polymer matrix (e.g., sulfonated poly (2,6-dimethyl-1,4-phenylene oxide) (sPPO)) led to synergistic effects of inorganic materials (e.g., high specific surface area, strong hydrophilicity, and facilitated conductivity, etc.) and those of organic materials (e.g., good chemical, thermal, hydrolytic stability, etc.) [63, 107, 108]. In addition, the O-MWCNTs-sPPO membrane also showed a simultaneous improvement in anti-fouling property and energy generation ability [108]. The further introduction of structural modification (porosity) to Fe_2O_3-SO_4^{2-}-sPPO membrane through two-step phase inversion resulted in a maximum power density of 1.4 W/m^2 [20]. Most

recently, a study on poly (arylene ether sulfone) (PAES) membranes containing three different cationic functional groups (i.e., 1-methyl-imidazolium (IMD), tetramethyl ammonium (TMA), and 1-azabicyclo[2,2,2]octane salt (ABCO)) demonstrated relatively low degree of swelling for IMD, resulting in membranes with simultaneously high permselectivity (i.e., 94.35-98.63 %) and considerable membrane conductivity (i.e., 1.65-3.86 Ω cm^2) [21].

Meanwhile, innovative fabrication methods (e.g., pulsed electric field used for preparing CEMs of aligned ion channels [65], radiation chemical grafting polymerization applied to make CEMs with various amounts of cross-linking agent [109]) have been used for making IEMs of ultra-low resistance (e.g., area resistance of 0.86 Ω cm^2). In parallel, membranes with tailored geometries (e.g., the inclusion of ridges, waves, pillars, and hemispherical protrusions [19, 67, 110]) have also been developed to eliminate the use of conventional spacers. Power density of 1.3 W/m^2 (corresponding to 38 % improvement over conventional membrane geometry) has been reported. More importantly, the introduction of microstructures decreased hydraulic friction in the water compartments (e.g., about 4 times lower pressure drop compared to custom membranes with spacers [19, 67]) and led to the allowance of using thinner flow channel spacing. Further details on spacerless RED membranes can be found in Section 4.2.2. Recent development in pore-filling membranes that consist of thin porous substrate and ion exchange polymer filled in the pores have been demonstrated as promising RED power density of 2.4 W/m^2 [64, 66].

423 **Table 1. Properties of commercial and tailor-made IEMs used in RED stacks**

Manufacturer	CEM	Materials	Supporting fabric	IEC (meq/g dry)	SD (%)	FCD (meq/g H_2O)	R^a (Ω cm^2)	α^b (%)	d (μm)	Typical power density (W/m^2)	References
Ionics Inc., USA	61CZL386	N.A.	N.A.	2.6	40	N.A.	9	N.A.	630	0.17	[25]
Asahi Chemical Industry Co. Japan	Aciplex K-501	Polyarylene, $-SO_3^{2-}$	N.A.	1.5	30-40	5.6	2~3	N.A.	180-200	0.130	[111]
Asahi Glass Co. Ltd., Japan	Selemion CMV*	PS/DVB, $-SO_3^{2-}$	PVC	2.01	20-30	6.8-10.1	2.29	98.8	101	1.65-1.8	[55, 66]
	Selemion CSO	PS/DVB, $-SO_3^{2-}$	PVC	1.04	16	6.4	2.26	92.3	N.A.	1.15-1.16	[63, 107]
Fujifilm Manufacturing Europe B.V.	CEM-80050-05	N.A.	N.A.	1.45	N.A.	N.A.	2.55	96	120	0.53-2.48	[3, 112-116]
	V1 CEM*	N.A.	N.A.	N.A.	N.A.	N.A.	1.6	93	125	0.7	[117]
Fuma-Tech GmbH, Germany	Fumasep FKD*	$-SO_3^{2-}$	PEEK	1.14	29	3.9	2.14	89.5	113	0.61-1.17	[55, 56, 60]
	Fumasep FKS*	$-SO_3^{2-}$	None	1.24-1.54	13.5-22	7.0-11.4	1.5-1.7	94.2-99	20-40	0.6-6	[20, 27, 66, 90, 118]
Tokuyama Co., Japan	Neosepta CMX*	PS/DVB, $-SO_3^{2-}$	N.A.	1.62-2	22-38	7.3	1.5-2.91	99	150	0.65-1.15	[57, 60, 67, 92]
DuPont, USA	NR-211*	Perfluorosulfonic acid/PTFE copolymer	N.A.	N.A.	50	N.A.	N.A.	N.A.	25.4	N.A.	[119]
PCA Polymerchemie Altmeier GmbH, Germany	PC-SK*	$-SO_3^{2-}$	Polyester	3	9	N.A.	2.5	95	160-200	0.3-0.8	[26, 120]
MEGA a.s., Czech Republic	Ralex CMH	$-SO_3^{2-}$	N.A.	2.34	31	7.54	11.33	94.7	764	0.55-1	[19, 39, 117, 121]
Shandong Tianwei Membrane Technology Co., Ltd. China	DF-120 CEMs	N.A.	N.A.	1.57	44	3.57	1.4	92	220	0.7	[32]
Hangzhou Qianqiu Industry Co., China	Qianqiu CEM*	$-SO_3^{2-}$	N.A.	1.21	33	3.7	1.97	82	205	0.5-1.05	[23, 60]
	KIER-CEM1*	Cross-linked N, N'-ethylenebis (acrylamide) and vinyl sulphonic acid	Porous polyolefin	2.64	26.9	9.8	0.34	97.8	26	2.4	[122]

Tailor-made	KIER-CEM2*	Cross-linked N, N'-ethylenebis (acrylamide) and acrylamido-2-methyl-1-propanesulphonic acid	Porous polyolefin	1.42	21.7	6.5	0.72	99.2	27	2.4	[122]
	MSC-X-Y*	PS/DVB, $-SO_3^{2-}$	PE	1.57-1.98	21.4-39.8	4.4-7.4	0.61-1.3	N.A.	120-147	3.56-4.32	[109]
	SPEEK 40*	Sulfonated polyetheretherketone, $-SO_3^{2-}$	None	1.23	23	5.3	2.05	95.3	53	~1-1.3	[96]
	SPEEK 65*	Sulfonated polyetheretherketone, $-SO_3^{2-}$	None	1.76	35.6	4.9	1.22	89.1	72	~1.13-1.25	[96]
	AC current aligned CEM*	sPPO, $-SO_3^{2-}$	None	0.91-1.06	N.A.	N.A.	0.86	96.2	80-91	1.34	[65]
	Organic-inorganic nanocomposite*	Fe_2O_3-SO_4^{2-} sPPO, $-SO_3^{2-}$	None	0.98-1.42	16-58	2.0-6.4	0.82-2.26	77.1-92.3	30-150	1.4	[20]
	Organic-inorganic nanocomposite*	O-MCNTs- sPPO, $-SO_3^{2-}$	None	1.77-2.28	36.9-42.6	N.A.	0.45-0.7	90-95.3	47-70	0.37-0.48	[123] [108]
	Organic-inorganic nanocomposite*	SiO_2–SO_3H sPPO, $-SO_3^{2-}$	None	0.78-1.49	15-34	2.6-9.9	0.85-1.87	79.1-94	30	0.8-1.3	[107]
	Hybrid organic film*	PVA-sPPO, $-SO_3^{2-}$	None	1.6-2.05	45-75	2.1-4.6	1.3-2.1	80-87	50	0.3-0.46	[94]

424

425

Manufacturer	AEM	Materials	Supporting fabric	IEC (meq/g dry)	SD (%)	FCD (meq/g H_2O)	R^a (Ω cm^2)	α^b (%)	d (μm)	Typical power density (W/m^2)	References
Asahi Chemical Industry Co. Japan	Aciplex A-201	N.A.	N.A.	1.4	25-28	5.38	3.6-4	N.A.	200-260	0.130	[111]
Asahi Glass Co. Ltd., Japan	Selemion AMV*	PS/DVB/Chloromethylstyrene, $-N(CH_3)_3^+$	PVC	1.78	17-19.8	9.0-10.5	3.15	87.3	107-124	1.65-1.8	[55, 66]
	Selemion ASV*	PS/DVB/Chloromethylstyrene, $-N(CH_3)_3^+$	PVC	N.A.	N.A.	N.A.	3.7	97	120	1.15-1.16	[63, 107]
Fujifilm Manufacturing Europe B.V.	AEM RP1 80045-01	N.A.	N.A.	1.28	N.A.	N.A.	1.83	96	120	0.53-2.48	[3, 112-116]
	V1 AEM*	N.A.	N.A.	N.A.	N.A.	N.A.	1.6	93	125	0.7	[117]
Fuma-Tech GmbH, Germany	Fumasep FAD*	N.A.	Polyester	1.42	34	4.2	0.89	86	74	0.61-1.17	[55, 56, 60]
	Fumasep FAS*	N.A.	None	1.12-1.5	8-23.5	4.8	0.5-1.03	89.4-95.5	20-36	0.6-6	[20, 27, 66, 90, 118]
Tokuyama Co., Japan	Neosepta AMX*	PS/DVB, $-N(CH_3)_3^+$	N.A.	1.25	16-17.5	7.1-7.8	1.03-2.35	90.7	129-134	0.65-1.15	[57, 60, 67, 92]
	Neosepta ACS*	PS/DVB, $-N(CH_3)_3^+$	N.A.	N.A.	N.A.	N.A.	3.5	N.A.	130	0.6	[55]
PCA Polymerchemie Altmeier GmbH, Germany	PC-SA*	$-NH_3^+$	Polyester	1.1	14	7.86	1.8	>93	180-220	0.3-0.8	[26, 120]
MEGA a.s., Czech Republic	Ralex AMH	N.A.	N.A.	1.97	56	3.5	7.66	89.3	714	0.55-1	[19, 39, 117, 121]
Shandong Tianwei Membrane Technology Co., Ltd. China	DF-120 AEMs	N.A.	N.A.	1.96	49	N.A.	2	98	250	0.17	[32]

Hangzhou Qianqiu Industry Co., China	Qianqiu AEM*	N.A.	N.A.	1.33	35	3.8	2.85	86.3	294	0.5-1.05	[23, 55]
Tailor-made	KIER-AEM1*	Cross-linked N, N-bis(acryloyl)piperazine and (vinylbenzyl)trimethylammonium chloride	Porous polyolefin	1.55	21.9	7.1	0.28	91.8	27	2.4	[122]
	PECH A*	Polyepichlorodydrin (PECH)-PAN, $-NR_3^+$	None	1.31	32.2	4.1	2.05	90.3	77	~1.06	[96]
	PECH B1*	Polyepichlorodydrin (PECH)-PAN, $-NR_3^+$	None	1.68	49	3.4	0.82	86.5	33	~1.25	[96]
	PECH B2*	Polyepichlorodydrin (PECH)-PAN, $-NR_3^+$	None	1.68	49	3.4	0.94	87.2	77	~1.13-1.25	[96]
	PECH B3*	Polyepichlorodydrin (PECH)-PAN, $-NR_3^+$	None	1.68	49.1	3.4	1.32	87	130	~1.06	[96]
	PECH C*	Polyepichlorodydrin (PECH)-PAN, $-NR_3^+$	None	1.88	53.5	3.5	1.14	79.2	77	~1.13	[96]
	PAES – ABCO*	Poly (arylene ether sulfone) (PAES), 1-azabicyclo [2,2,2] octane (ABCO)	None	1.2-1.48	11-17	10.55-12.62	1.59-3.82	93.53-97.23	66-70	1.16	[21]
	PAES – IMD*	Poly (arylene ether sulfone) (PAES), 1-methyl-imidazolium (IMD)	None	1.19-1.48	8-13	13.31-16.4	1.65-3.86	94.35-98.63	59-64	1.2	[21]
	PAES – TMA*	Poly (arylene ether sulfone) (PAES), basic tetramethyl ammonium (TMA)	None	0.97-1.69	6-50	6.68-9.06	1.45-3.53	91.56-96.56	58-70	1.14	[21]

[a] Membrane resistance measured in an electrolyte solution of 0.5 M NaCl solution at 25 °C.

[b] Membrane permselectivity measured under a concentration difference of 0.5 M NaCl and 0.1 M NaCl solution at 25 °C.

[C] The presented value is based on theoretical calculation instead of experimental result.

*Membranes have homogeneous structures.

N.A.: Specific information not reported in the original study.

4.2. Spacers

4.2.1. Effects of spacer on RED performance

Spacers are commonly used in RED stacks for supporting IEMs, providing flow channels, and promoting mixing [121]. Enhanced mixing tends to minimize concentration polarization and thus reduce non-ohmic resistance [124]. At the same time, the presence of non-conductive spacers reduces active membrane area for ionic conduction (which is also known as the spacer shadow effect) and makes ionic transport path more tortuous, resulting in higher ohmic resistance particularly in LS compartments [18, 52]. In addition, pumping solutions through spacer-filled channels can be a major source of energy loss (e.g., 25 % of energy generated) due to the significant pressure drops (particularly for thinner channels) [60, 90, 125]. The substantial impacts of spacers depend largely on spacer materials and geometry [18, 52, 60, 126].

In RED, the spacer thickness can play a critical role in the power output performance since it directly affects the electrical resistance of the solution compartments. In particular, it has been well recognized that LS compartments usually have major contribution to the overall internal resistance [18, 90]. Owing to the relatively low electric conductivity of LS. Thus, thinner spacers are often preferred for reducing internal resistance of an RED stack [18, 24, 54, 57, 59]. Recent studies demonstrated an improvement in power density by a factor of 1.6 (correspondingly from 0.56 W/m^2 to 0.87 W/m^2) by simply reducing spacer thickness from 0.5 mm to 0.2 mm [18, 57]. Using a spacer thickness of 0.1 mm, Vermaas et al. [90] reported a power density of as high as 2.2 W/m^2. Nevertheless, the use of overly thin spacers can significantly increase energy consumption for pumping due to greater pressure drop in the flow channels, which reduced the available net power density (i.e., the gross power density – power for pumping). Thus, the high energy consumption for pumping makes ultrathin feed spacers

(e.g., 0.06 mm) impractical for RED applications [25, 90, 121]. In addition, small spacer thickness tends to be more vulnerable to fouling, thus leading to reduced stability of stack operation in practice. Spacer thickness needs to be carefully optimized to achieve a maximized net power density [12, 18, 37, 57, 60, 61, 90, 127, 128]. It is also worth to be noted that the specific value of optimal spacer thickness varied with other parameters of an RED stack. For example, a spacer with greater open-area (which is less prone to pressure drop) favors a thinner spacer thickness.

4.2.2. Novel spacers designs

For a typical lab-scale RED stack using non-conductive spacers, the shielding effect might increase internal resistance by a factor of 1.5 [60] and possibly contribute to 30-40 % less energy generation compared to the theoretically available energy [57]. Długołęcki et al. explored the use of ion-conductive spacers in order to eliminate the spacer shadow effect, and their study demonstrated 3-4 times enhancement in power density [52]. Researchers have also developed spacers with greater open area in order to reduce the shielding effect [60, 66]. In addition, such spacers tend to significantly reduce the hydraulic friction in the flow channels and thus allow the use of thinner channel gap (say ~ 100 μm or less) to achieve reduced electrical resistance [19, 90]. An interesting concept of profiled membranes has been proposed in the recent literature. These novel RED membranes, also termed as "spacerless membranes", are designed with tailored microstructures (e.g., ridges, waves, pillars, and reliefs, see Fig. 10 (i)-(iii) and Section 4.1.3) that avoid the use of spacers [19, 67, 110]. The reduced pressure drop together with the lower overall electrical resistance improves the RED power output (e.g., 10 % and 20 % higher net power densities using a ridge- and pillar-structured membranes respectively, despite the increased concentration polarization [19]). Other spacer geometries, such as twisted spacers or profiled membrane added with sub-corrugations, have also been

reported [121]. Recently, Pawlowski et al. demonstrated that profiled membranes with integrated chevron structures showed low hydraulic friction and simultaneous efficient fluid mixing [129, 130] (Fig. 10 (iv)). Some recent studies have also reported the use of ion exchange resin (e.g., packed resin beads confined in LS compartments) for avoiding spacers and enhancing ionic transport in LS compartments, though this approach typically requires relatively large inter-membrane distance (i.e., 500 µm) [68, 131].

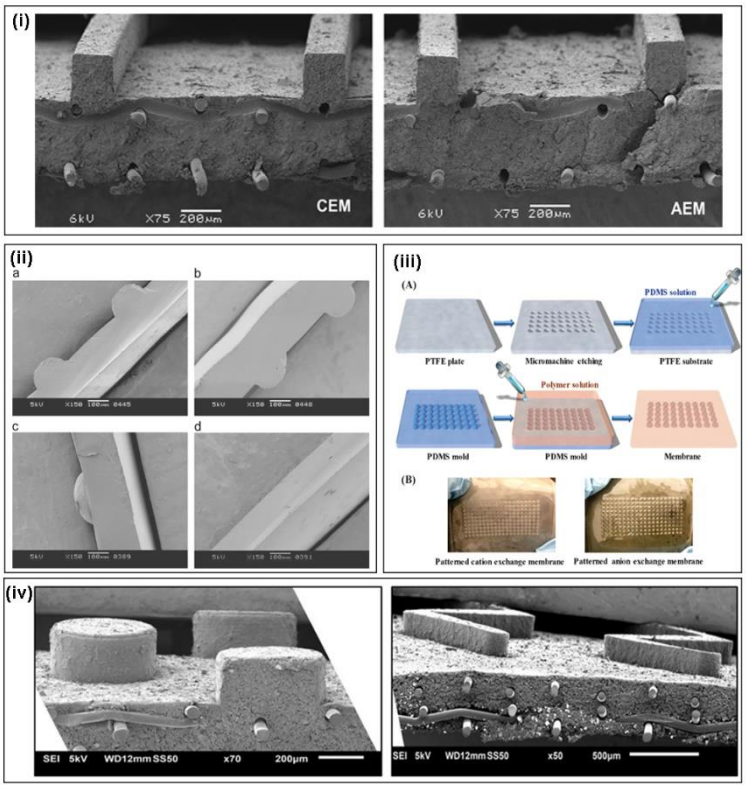

Fig. 10. Scanning electron microscope (SEM) images of (i) profiled CEM and AEM with ridge structures (figure is taken from [19] with copyright permission from Elsevier), (ii) micro-structured AEM with ridge, wave, pillar structures vs. a conventional flat AEM (figure is taken from [67] with copyright permission from Elsevier), (iii) patterned CEM and AEM with hemispherical protrusions (figure is taken from [110] with copyright permission from Elsevier), and (iv) profiled AEM with pillar and chevron corrugations (figure is taken from [130] with copyright permission from Elsevier).

In addition to spacer geometry, it is also critical to ensure uniform feed flows distribution by modifying water feeding pattern (e.g., wider feed manifolds, additional water inlet and outlet, etc.) [23, 126, 132], which could result in as much as 36.4% higher net power density [23]. Further studies on feed fluid flow patterns in water compartments suggested that short flow path [6, 88, 125, 128, 132-134] and co-current flow (compared to counter-flow) of feed water flow [125, 134] are both preferred for high net power density. Recently, a novel breathing cell with rhythmically tunable intermembrane distance (e.g., periodically compressing LS compartments while expanding HS compartments) realized the reduction of inter-membrane distance of LS without increasing the pumping energy consumption, resulted in a net power density of 1.3 W/m^2 [118].

4.3. Electrode systems

Electrode systems, comprising electrodes and electrolytes filled in the electrode compartments, convert ionic current to electric current through redox reactions. The most commonly used electrode systems can be classified into two categories: with or without opposite electrode reactions [135]. The latter ones usually involve gas formation (e.g., H_2, Cl_2 or O_2 generation) redox reactions (e.g., water splitting) [25, 50]. Such electrode systems generally feature high voltage losses for gas generation and additional devices are needed for the collection of toxic (e.g., Cl_2) and/or explosive gases (e.g., H_2) [135-137]. In order to improve power generation performance and to ensure safety, electrode systems with opposite reactions are more frequently used, in which no net chemical reactions take place [135]. Such electrode systems can be further divided into two sub-groups: systems with reactive electrodes (e.g., Cu-$CuSO_4$ system [43] and Zn-$ZnSO_4$ [50]) and systems with homogeneous redox couples (e.g., $FeCl_3/FeCl_2$, $[Fe(CN)_6]^{3-}/[Fe(CN)_6]^{4-}$ and Fe(III)-EDTA/Fe(II)-EDTA) [136] with inert electrodes (e.g., titanium mesh coated by Ru-Ir metal oxide electrodes, graphite electrodes, etc.)

[136, 138]. A major disadvantage of reactive electrodes is the requirement of periodical change of feed solutions and inversion of electric current [135, 136]. Therefore, inert electrodes with homogeneous redox couples are preferred. The corresponding reversible redox species and electrode materials were both studied on their properties and the impacts on RED performance [135, 136, 138]. Compared to most commonly used precious metal oxide electrodes, carbon electrodes may be favored for iron based redox couple, due to their high over potential for gas evolution [135]. Burheim et al. further suggested that low-cost carbon electrodes might substitute traditional noble metal oxide electrodes [138]. A recent study reported that a 5-10 % improvement of power density would be realized by using porous carbon black coated graphite foil compared to conventional metal mesh electrodes [22]. Besides, increasing specific surface area of the custom-made electrodes can achieve further improvement [22]. Nevertheless, it is worth to be noted that iron based redox couples can potentially poison the outer IEMs or form iron precipitates [135]. Although energy dissipation on the electrodes is inevitable, its impact can be minimized by using a large number of cell pairs in an RED stack (e.g., 50 – 500) [1, 19, 42].

5. Effects of operation conditions on RED performance

5.1. Feed solutions properties

The feed solutions determine the electromotive driving force (Equation 2) and contribute to the internal resistance (Equation 5). In particular, the dilute salt solution of low conductivity in LS compartments is a major contributor to the overall internal resistance (e.g., LS may account for up to 45 % of overall internal resistance when seawater and river water were used) [4, 5, 27, 59, 60, 116, 139-141]. Seawater (~ 3 %) and river water (typically 0.05-0.1 %) are most commonly reported feed solutions (Fig.11), because of their easy accessibility [18, 37, 89, 134]. Synthetic solutions, mostly of NaCl, are commonly used for lab-scale evaluation. Alternative

HS and LS sources have also been explored. Majority of the alternative HS have higher concentration (often > 5%) than typical seawater to achieve better RED power output performance. Examples of HS include brine from seawater desalination facilities [2, 27, 140, 142], hypersaline solutions (e.g., Dead Sea water) [4, 61, 116, 143], and synthetic high concentration solutions used for closed-loop osmotic heat engine [5, 26, 30] (see further details in Section 6.1). Alternative LS solutions include brackish water and treated wastewater (0.1-3 %) [1, 29]. Fig. 11 summarizes the power density reported in the recent literature for various combinations of HS/LS.

A series of studies have been conducted to investigate the effect of feed solution concentrations on RED power generation. In general, RED performance can be enhanced by higher HS concentration as well as greater salinity difference between HS and LS. For example, the power density can be increased by approximately ten times by increasing the HS concentration from 0.5 M to 5 M [12]. Daniilidis et al. reported a power density of as high as 6.7 W/m^2 using fresh water (0.01 M NaCl) and concentrated brine (5 M NaCl) at 60 °C [4]. However, membrane permselectivity tends to decrease in concentrated brine, which would limit further improvement of power generation [4].

For a given HS, higher LS concentration results in two competing effects: reduced electromotive force that would reduce power output performance and lower internal resistance that would promote greater power density [26, 27, 144]. In addition, higher LS concentration decreases concentration polarization and reduces non-ohmic resistance [145]. Thus, careful optimization of the LS concentration is required to achieve the maximum power density. Mei et al. [144] reported an optimal LS concentration in the range of 5-20 mM. According to their study, lower LS concentration led to excess power loss over the increased internal resistance,

while higher LS concentration resulted in substantial reduction in the available electromotive force. It is important to note that the optimal LS concentration depends on the properties and operation of the RED system. For example, low LS concentration can be better tolerated in RED stacks featuring thinner LS channel thickness; for such conditions, the electrical resistance of the LS compartments would play a less importance role [27].

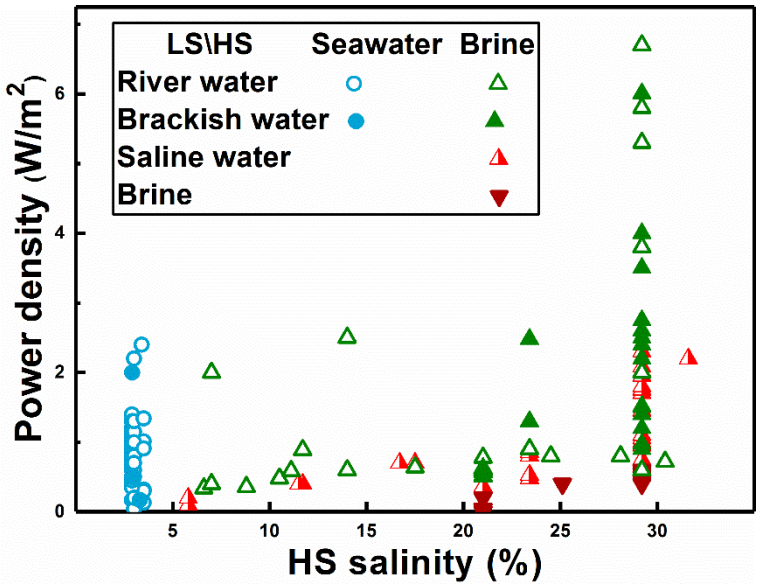

Fig. 11. RED power density reported in recent literatures for varying HS/LS pairs. In each pair, the salinity level of the low salinity stream is represented by different marker shapes, and the salinity level of the high salinity stream is shown in x axis. The salinity range of river water is below 0.1 %, brackish water is 0.1 – 3.0 %, saline water is 3.0 – 5.0 %, and brine is above 5.0 %. The data are obtained from Scopus and Google Scholar databases by September 2017. Keyword for searching is 'reverse electrodialysis'.

Several studies have also investigated the influence multivalent ions (e.g., Mg^{2+}, SO_4^{2-}, etc.), which are ubiquitous in natural water sources, on RED performance [112, 116, 117, 146]. The results suggested that the presence of multivalent ions in feed solutions tends to increase the membrane resistance and thus lowering power output performance [147]. Besides, multivalent ions would transport from LS to HS (also known as up-hill transport) in the sacrifice of two times the amount of monovalent ions transport from HS to LS, leading to reduced voltage

590 output [117, 148]. This phenomenon takes place when the multivalent ions only exist in LS
591 and when multivalent ions are presented on both sides of solutions that electrochemical motive
592 force of multivalent ions and monovalent ions are different [24, 50, 117, 137, 146, 147]. When
593 using natural water as feed solutions, these combined effects of increased resistance and
594 decreased voltage output could lead to ~ 50 % decrease in power density compared with that
595 obtainable using synthetic solutions [37]. In order to eliminate up-hill transport of divalent ions
596 against the overall concentration gradient, monovalent ion selective membrane is preferred
597 [147, 148]. Güler et al. [148] prepared a highly negatively charged layer on a commercial AEM
598 by copolymerization of 2-acryloylamido-2-methylpropanesulfonic acid with N,N-
599 methylenebis (acrylamide), and the resulting membrane showed greatly reduced transport of
600 multivalent ions [148]. An added advantage of the membrane was the improved hydrophilicity
601 and anti-fouling ability. Additional measures, such as softening pretreatment and combining
602 higher flow rate of HS with thicker compartment channels, have also been investigated [116,
603 146].
604
605 **5.2. Feed flow velocity and temperature**
606 Increasing flow velocity of feed solutions would improve ionic mixing in water compartments
607 (which reduces non-ohmic resistance) and increase electromotive force at the expense of more
608 pumping energy (See Section 4.2.2 and [57, 58, 120, 127, 134, 145]). Furthermore, higher flow
609 velocity can effectively minimize the effect of increased LS concentration due to the
610 accumulation of ions transported from HS to LS [120]. Therefore, there is an optimal flow
611 velocity for maximizing the net power density [57, 60, 115, 134, 149] (Fig.12). This optional
612 value would depend on the stack design (e.g., channel thickness and spacer geometry) and
613 operation conditions (e.g., feed solution concentration) [127, 149]. For lab-scale RED tests, a
614 flow velocity on the order of 1 cm/s is often recommended [27]. It is worthwhile to note that

the optimal flow velocity of LS may differ from that of HS. Since the contribution to the total electrical resistance by the HS is generally less important, a lower flow velocity can be adopted for HS to decrease its pumping energy [127]. For LS (e.g., fresh water), the optimal flow velocity was determined by the competing effects of increasing concentration polarization and decreasing electrical resistance, as well as pumping energy consumption [27, 120]. The optimal flow velocity of LS would be higher than that of HS since the electrical resistance of the LS is often orders of magnitude larger compared to the resistance of the HS.

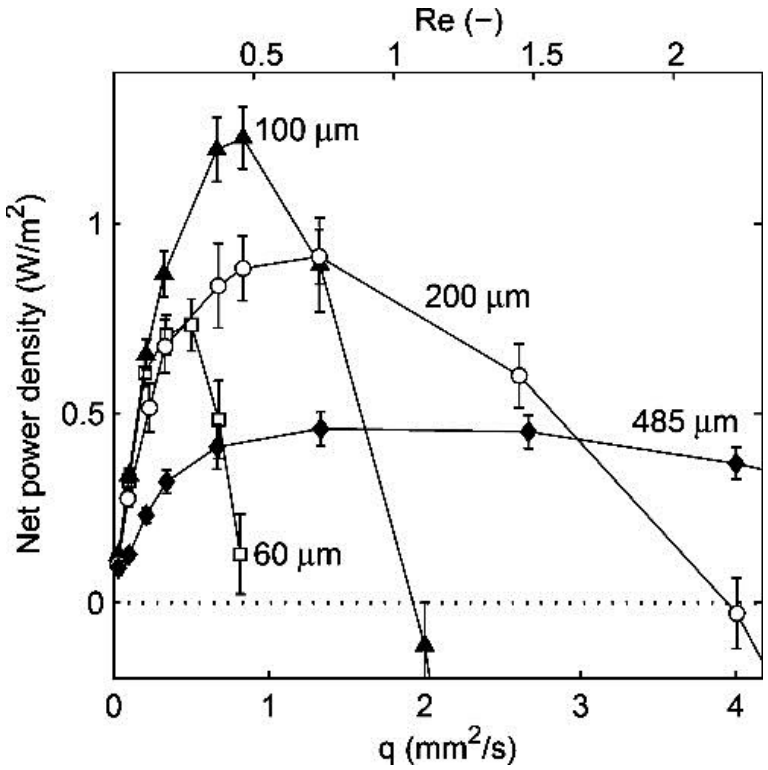

Fig. 12. The correlation between maximum net power density and flow velocity. The flow velocity is reported per cell per unit width, i.e., flow rate per cell divided by the cell width. Figure is obtained from reference [90] with copyright permission from ACS Publications.

Temperature of feed solutions also needs to be taken into consideration because of its importance influence on electromotive force and conductivity of both solutions and IEMs [27, 57, 142]. Fig. 13 shows a correlation between RED power density and feed solution

temperature. Since temperature of natural water sources can have significant seasonable and diurnal variations, which might have considerable influences on RED performance [4, 57, 59, 144]. Water sources with high temperatures (e.g., solar heated desalination brines [59, 150], membrane distillation effluents [115], and heated synthetic thermolytic solutions [5, 30]) are beneficial to RED power production. However, excessive high temperature of feed solutions may affect membrane permselectivity. Daniilidis et al. [4] reported a reduced permselectivity of 68% at 60 °C. On the other hand, Mei [144] showed that greatly enhanced power performance at 60 °C. In order to fully harness the benefit of warm brines, more thermally resistant RED membranes are desirable.

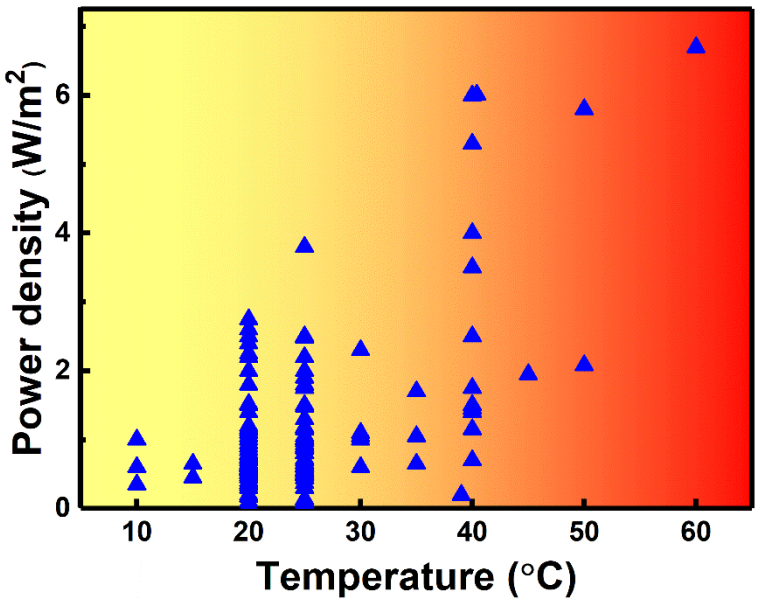

Fig. 13. The correlation between temperature of feed solutions and power density reported in recent publications. The data are obtained from Scopus and Google Scholar databases by September 2017. Keyword for searching is 'reverse electrodialysis'.

5.3. RED fouling

Fouling is one of the key bottlenecks for the practical implementation of RED. The use of natural water sources can result in fouling of both membranes and spacers in an RED stack.

649 Fouling can significantly reduce power density (e.g., 60 % decrease using natural seawater and
650 natural river water [37]) as a result of increased resistance and decreased apparent
651 permselectivity [37, 151]. The type and rate of fouling are significantly affected by the fixed
652 charges on the membrane surface. For example, negatively charged CEMs tend to be sensitive
653 to scaling. In contrast, positively charged AEMs are more prone to organic fouling and
654 biofouling [37, 38]. Spacers can also play a critical role in fouling formation in water
655 compartments. A recent study reports that spacers were more vulnerable to biofouling than
656 membranes [19]. In this regard, spacerless RED stacks using profiled membranes can achieve
657 reduced fouling; Vermaas et al. observed a 40 % decrease in power density for profiled
658 membrane compared to 60 % decrease for conventional membranes [37]. In addition, the
659 location of foulant (i.e., in HS vs. in LS) would also determine its impact on RED performance
660 [151]. Kingsbury et al.'s work suggested that RED stack with natural organic matter presented
661 in LS tends to be more sensitive to fouling.
662
663 Various strategies have been explored for fouling control in the context of RED. Some
664 important examples include optimization of operational conditions [39], improved spacer
665 design [23] and membrane surface modification [38]. Periodic feed solutions interchange (i.e.,
666 switching the flow compartments of HS and LS) combined with periodic air sparging has been
667 shown to be effective to prevent both of organic fouling and colloidal fouling [39]. Recently,
668 Moreno et al. applied CO_2 saturated feed solutions for fouling mitigation and showed better
669 result than air sparging due to bubble nucleation [152]. Spacers providing more uniform flow
670 distribution is less prone to fouling [23]. Membrane surface modification is another promising
671 way for fouling control. Some studies showed obvious enhancement in fouling resistance for
672 AEMs coated with a hydrophilic positively charged layer [38, 148]. A recent study reported
673 the preparation of anti-fouling nanocomposite CEMs by incorporation of carbon nanotube

[108]. Nevertheless, compared to the vast literature [153, 154] on antifouling membrane modification in the literature on pressure-driven water filtration membranes, studies on RED membrane modification are still limited.

6. Novel RED process development

Within last decade, versatile combinations of RED with different technologies substantially extend the application scope of RED. For instance, a closed-loop RED heat engine, which integrates RED with a thermal-based solution separation process (e.g., distillation process) for regenerating the feed solutions used in RED, can be used to convert low-grade heat (≥ 40 °C) to electricity [5, 7, 155]. The combination of RED with bio-electrochemical fuel cell (i.e., microbial RED cell) can avoid electrode reactions of high overpotential in RED stack and boost power production of bio-electrochemical fuel cell [28, 30, 31]. Co-location of RED with different desalination processes (e.g., reverse osmosis, ED, and capacitive deionization, etc.) have been demonstrated to enhance RED power generation and simultaneously eliminate the negative effects of brine effluent of desalination facilities [29, 32-34, 144, 156].

6.1. Closed-loop RED heat engine

Synthetic solutions that can be easily regenerated by low-grade heat are promising alternatives to natural water sources, which enables closed-loop RED heat engine for the conversion of thermal energy to electricity [5, 7]. The use of synthetic solutions in a closed-loop also avoids the need to extensively pretreat feed solutions, overcomes the limitation of accessibility to natural water sources, as well as minimizes membrane fouling [1, 30, 139]. A typical closed-loop RED heat engine (also known as thermal energy driven electrochemical generator) is consisted of two working processes [1, 5] (Fig.14): the first step converts the SGP between two synthetic solutions of different concentrations into electricity in an RED stack; in a second step,

699 a thermal based separation unit is then used to regenerate the synthetic solutions that can be
700 recycled back to the RED stack. RED heat engine was first reported by a thermolytic
701 ammonium bicarbonate as the HS, which demonstrated a maximum power density of 0.33
702 W/m^2 [5]. In such RED stack, short vertical flow path and improved spacer geometry could
703 benefit the power performance by reducing membrane area shielded by gaseous bubbles (CO_2
704 and NH_3) released from the thermolytic solution and decreasing concentration polarization [6].
705 Further investigations on the optimization of operation conditions (e.g., greater concentration
706 difference, higher flow rate of feed solutions) and stack geometry design (e.g., optimal
707 compartment thickness) have also been conducted [7, 113, 157, 158]. Membranes optimized
708 for thermolytic feed solutions are required. A recent work by Geise et al. shows that IEMs with
709 higher swelling tendency in ammonium bicarbonate tends to achieve better power density using
710 ammonium bicarbonate powered RED [155]. Further coupling of thermolytic solution with a
711 microbial RED cell (MRC, see more details in Section 6.2) resulted in an RED power density
712 of 0.5 W/m^2 (or 5.6 W/m^2 when normalized to cathode surface area, which was about five times
713 higher than that obtained from only MFC) [30]. Similarly, incorporation of thermolytic solution
714 with microbial RED cell with biogas production (e.g., hydrogen or methane) was also
715 investigated [139, 159, 160].
716
717 So far, the most widely reported solutions for closed-loop RED heat engine is the thermolytic
718 ammonium bicarbonate. Nevertheless, simple solutions such as NaCl can also be used in
719 closed-loop RED heat engine, e.g., by using membrane distillation for its regeneration [115].
720 Future studies are needed to explore a great range of feed solutions for RED heat engine.
721

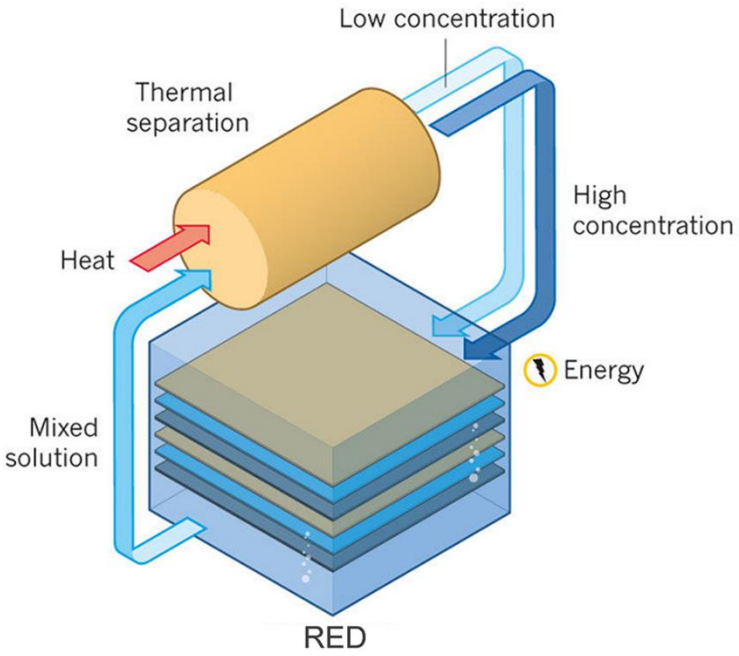

Fig. 14. Schematic diagram of a typical closed-loop RED heat engine that comprises an RED stack and thermal driven separation unit. Figure adapted from reference [1] with copyright permission from Springer Nature.

6.2. Microbial RED cell

Microbial RED cell is an interesting hybrid process that overcomes limitations of individual process [31]. Table 2 summarizes the key properties of microbial RED cells reported in recent literatures. Particularly, thermodynamic favorable electrode reactions (i.e., anodic oxidation of organic matter by exo-electrogenic bacteria and cathodic reduction of oxygen [30, 31]) produce additional voltage to RED and avoid overpotential of conventional electrode reactions (e.g., 1-2 V voltage loss for a 25 cell pairs RED stack [55]). The first experimental study on microbial RED cell with five pairs IEMs obtained a maximum voltage output and power density (normalized to cathode surface area) of 1.3 V and 4.3 W/m^2, respectively, using acetate fuel and sodium chloride solutions [31]. Several measures have also been explored to further increase microbial RED cell performance. The adoption of profiled membranes with hemispherical protrusions avoided using non-conductive spacers and increased the power density from 2.5 W/m^2 to 3.44 W/m^2 (normalized to cathode surface area) [110]. In addition,

739 reducing RED membrane pairs have been demonstrated to contribute to high power density
740 (e.g., increased from 0.5 W/m^2-membrane area to 3.1 W/m^2-membrane area when decreasing
741 membrane pairs from 5 to 1, using acetate fuel) and reduced the capital costs [161]. In microbial
742 RED cells, the electrode reactions provide spontaneously additional voltage output (e.g., 0.5 –
743 0.8 V) to RED [31, 161]. The boosted voltage output of hybrid process could be used for driving
744 cathodic chemical evolution (e.g., hydrogen, acid and alkali, methane, hydrogen peroxide) [28,
745 159, 160, 162-168], and for pollutants (i.e., azo dye, Cr (VI)) abatement [167, 169]. The
746 incorporation of thermolytic solution into these hybrid systems (Section 6.1) further increased
747 the power density and eliminated the need of natural water sources and reduced the capital cost
748 of pre-treatment [30, 139, 159, 161, 170].
749

750 **Table 2. The summary of hybrid processes of RED and bio-electrochemical processes in reviewed literatures.**

Hybrid process type	FS[a] of microbial compartment	FS of membrane stack	Flow velocity in membrane stack (cm/s)	Number of membrane stack cell pairs	P_d[b] (W/m^2)	Energy efficiency (%)	Chemical production	References
MREC	1 g/L CH_3COONa +phosphate buffer	0.6 M /0.012 M NaCl	~0.001-0.01	5	N.A.	64 %	0.8-1.6m^3 H_2/m^3 anolyte/day	[28]
MRC	1 g/L CH_3COONa +phosphate buffer	0.6 M /0.012 M NaCl	~0.01-0.02	5	3.6-4.3	N.A.	None	[31]
MRC	1 g/L CH_3COONa	1.1 M/0.011 M NH_4HCO_3	~0.02	5	5.6	~32	N.A.	[30]
MRC	1 g/L CH_3COONa +nutrient buffer	1.4 M/0.014 M NH_4HCO_3	0.01	5	N.A.	22	~3.1 mol H_2/mol acetate	[139]
MRC	2 g/L CH_3COONa+buffer	1.0 M/0.01 M NH_4HCO_3	0.08	2	4.2	N.A.	N.A.	[161]
MRC	Wastewater	1.0 M/0.01 M NH_4HCO_3	0.08	2	1.9	N.A.	N.A.	[161]
MREC	1 g/L CH_3COONa+nutrient buffer	1.7M /0.023M NH_4HCO_3	0.01	5	N.A.	27	3.5 mol H_2/mol acetate	[160]
MRCC	1 g/L CH_3COONa+nutrient buffer	0.6 M /0.012 M NaCl	0.02	5	0.908	N.A.	1.35 ± 0.13 mmol Acid and 1.59 ± 0.14 mmol alkali	[165]
MRC	1 g/L CH_3COONa +nutrient buffer	0.6M/0.006M NaCl	0.025	2	3.44 ± 0.02	34 ± 1	N.A.	[110]
MRMC	1 g/L CH_3COONa +nutrient buffer	1.7M /0.023 M NH_4HCO_3	0.008	6	N.A.	7.0 ± 0.3	0.6 ± 0.01 mol CH_4/ mol acetate	[159]
MRECC	0.82 g/L CH_3COONa+nutrient buffer	0.6 M/0.006 M NaCl	0.014	7	0.377 ± 0.023	N.A.	0.45 ± 0.01 mmol Acid, 1.09 ± 0.02 mmol alkali, and 10.3 ± 0.7 Ml H_2	[168]
MRC	LB broth	5 M/0.01 M NaCl	0.23	7	0.01	N.A.	Cr(VI) abatement	[169]
MREC	Fermentation wastewater	1.4M NH_4HCO_3/ DI water	1.25	10	N.A.	N.A.	1.1 ± 0.1 L H_2/g COD	[162]

MREC	1.0 g/L CH_3COONa + 0.1 M PBS	0.517 M /0.010 M a mixture of NaCl and $MgSO_4$	N.A.	7	N.A.	N.A.	1.32-1.71 mol H_2/mol COD	[163]
MREC	A mixture of CH_3COONa, NH_4Cl, and $NaH_2PO_4 \cdot 2H_2O$	0.6 M/0.012 M NaCl	0.037	10	N.A.	N.A.	0.51 mol H_2/mol COD	[164]
MREC	0.02 M 0.02 M CH_3COONa+domestic wastewater	0.6 M/0.006 M NaCl	N.A.	5	N.A.	N.A.	11.5 ± 0.5 mg H_2O_2/ L·h	[166]
MREC	0.02 M 0.02 M CH_3COONa+domestic wastewater	0.6 M/0.006 M NaCl	N.A.	5	N.A.	N.A.	0.4 g/L Orange G abatement	[167]

Abbreviations: MREC, microbial reverse-electrodialysis electrolysis cell; MRC, microbial reverse-electrodialysis cell; MRCC, microbial reverse-electrodialysis chemical-production cell; MRMC, microbial reverse-electrodialysis methanogenesis cell; MRECC, microbial reverse-electrodialysis electrolysis and chemical-production cell.

[a] FS represents the feed solutions.

[b] P_d represents the power density per m^2 cathode area.

N.A.: specific information not reported in the original study.

6.3. Hybrid process for desalination/energy storage

Co-localization of RED and desalination facilities is another promising direction [144]. In such hybrid systems, RED converts salinity gradient power to electricity that can be used to power up a desalination facility or offset its energy consumption [29, 32-34, 156]. At the same time, the concentrated brine from the desalination plant can be used as a HS with higher salt content compared to seawater. As a result, greater power generation can be achieved; the RED treatment reduces the concentration of the brine and minimizes its environmental and ecological impacts (e.g., density plume formation [29]). Brauns et al. first proposed the idea of further concentrating desalination brine using solar energy before feeding to an RED system [51, 59]. Li et al. developed a mathematical model to investigate the synergistic hybridization of RED with reverse osmosis desalination [29]. Their results show shat using either RED post-treatment of RO brine or RED pre-treatment of RO feed can result in dramatic energy savings in desalination [29]. RED can also be integrated with capacitive mixing to achieve simultaneous energy harvest and pure water production; a recent study reported a power density of 0.26 W/m^2 by recovering SGP of the two discharged streams from capacitive mixing (e.g., 0.017 M NaCl and 0.5 M NaCl) [156, 171]. A series studies have been conducted on combining RED and ED in different configurations [32-34]. It has been demonstrated that using RED as a pretreatment to ED would reduce concentration difference of feed solutions and thus energy saving in the ED step can be obtained [34]. Produced energy in the RED can also partially compensate the energy consumption in ED process; even energy self-sufficient desalination can be possibly realized in the hybrid systems [32, 33].

Other alternative SGP energy utilization and storage technologies have received increasing attentions. There have emerged several interesting hybrid systems, in which RED severed as the power source of co-located processes (e.g., alkaline water electrolysis cell for hydrogen

production, reverse osmosis in a sustainable greenhouse system and flow battery for energy storage) [172-174]. Meanwhile, innovative applications of RED as an energy storage device by operating it in a round cycle (i.e., charging step followed by discharging step) has also been explored [8, 9, 69].

7. Future perspectives

Pilot studies, which plays critical role in bridging lab-scale testing to full scale implementation, are still lacking. Section 7.1 summarizes the existing pilot plants in the Netherlands [71] and Italy [3, 42]. Additional pilot-scale studies are needed to enable the scaling up of the RED technology. Another key bottleneck of the RED technology is the limited power density available. At the same time, novel nanofluidic/microfluidic RED membranes using ion selective nanofluidic channels or nanopores show power density of orders of magnitude higher than conventional ion exchange membranes [35, 175-178]; the latest development are summarized in Section 7.2.

7.1. Pilot testing

Pilot testing is a critical step to enable large-scale implementation of RED. To date, there are only handful number of RED pilot plants reported in the literature, which are situated in the Netherlands [71] and Italy [3, 42], respectively. In 2014, the Netherlands commissioned the first RED pilot plant at Afsluitdijk, which features a 32 Km long dyke separates the IJssel Lake from the Wadden Sea. Electrical energy was produced from controlled mixing fresh water (0.02-0.05 %) with seawater (~2.8 %). Unfortunately, the operational data of the plant is not available to the public.

Detailed pilot operation has been documented for the pilot studies in Italy. An RED pilot plant was commissioned next to the Ettore-Infersa saltworks in Trapani (Italy) using saturated brine (~23.4-29.2 % NaCl equivalent) from the adjacent saltworks and brackish water (~0.18 % NaCl equivalent) from a shoreline well nearby. An overall power output of 40 W was reported for the plant with a total membrane area of 50 m^2 (by 125 cell pairs with a 44×44 cm^2 membrane area), corresponding to an averaged power density of approximate 0.8 W/m^2. No substantial performance decline occurred over a five-month operation. In 2016, this pilot plant was further scaled up by adding two RED unit which comprised 500 cell pairs of 44×44 cm^2 membrane area each (i.e., 400 m^2 of IEMs) [42]. The resulting power output was 330 W, with a power density of approximately 0.83 W/m^2. This value was about 50 % less than the power density obtained with synthetic NaCl solutions were used, mainly attributed to relative large concentration of bivalent ions (e.g., Mg^{2+}, SO_4^{2-}) in the concentrated brine [42]. Since pre-treatment for removing multivalent ions can be costly, the pilot test results revealed the importance of developing monovalent ion selective membranes to eliminate these impacts of bivalent ions (see detailed discussion in Section 5.1).

Despite the few pilot studies mentioned in this section, most of the existing plants are of limited capacity (up to 330 W). The generally low power density (< 1 W/m^2) obtained in these existing pilot studies highlight the critical need to develop novel RED membranes with greatly improved power performance. Larger scale pilot plants, coupled with full life cycle cost analysis, are needed to further validate the feasibility of RED.

7.2. Nanofluidic/microfluidic RED (nRED/μRED)

Several recent studies explored SGP harvesting using nano-/micro-fluidic devices with uniform channel or pore structures [35, 63, 175, 179-182]. Table 3 summarizes the reported power

density of nRED/μRED in recent literatures. In 2010, Guo et al. reported a nanofluidic SGP harvesting system using a single ion-selective track-etched nanopore embedded in polyimide membrane and produced a power output of 26 pW [35]. It was estimated that the porous membrane with a pore density of 10^8-10^{10} cm^{-2} could achieve a power density of 1-3 orders of magnitude higher (i.e., 20-2600 W/m^2) over traditional IEMs [35]. This result can be further improved by better engineered geometry and surface chemistry of the nanopores as well as the choice of electrolyte types [36, 183]. To avoid swelling or shrinking of organic membrane in electrolytes, Kim et al. established an inorganic nRED with silica nanochannels and obtained a power density of 7.7 W/m^2 [175, 184]. In order to overcome the difficulty in fabricating membranes with high pore density in large scale, anodic porous alumina was also explored [176]. It has packed nanopores with uniform pore radius over the range of 4-200 nm. Adding a dense silica layer to the surface of this porous alumina substrate substantially increase the anti-fouling ability [185]. Packing of self-assembled silica nanoparticles, which is facile and easy to scale up, can provide ion-selective nanochannel networks by the nanoparticle interstice [179, 186, 187]. Recently, Guo's research group proposed a smart synthetic 2D nanofluidic energy harvesting system by oppositely charged graphene oxide membranes pair [188]. They obtained a high voltage of 2.7 V and 54 % higher power density over commercial IEMs. Meanwhile, it was found that the hydrodynamic slip on the surface of nanochannels contributed to high power generation [180, 189]. The operation conditions (e.g., concentration difference, operation temperature) and geometric design of nanofluidic channels/nanopores (e.g., nanochannels/nanopores radius and length) have also been investigated [181, 190, 191]. There were several emerging novel nRED/μRED systems. For example, a hybrid membrane device fabricated by grafting a porous BCP (block copolymer) membrane onto a track etched PET (polyethylene terephthalate) substrate have conical nanochannels [177]. A power density of 0.35 W/m^2 was achieved using 0.5 NaCl and 0.01 M NaCl as feed solutions. Other interesting

855 investigations include paper based microfluidic RED in which feed flows was driven by
856 capillary without energy consumption [119], charged polyelectrolytic ion exchange polymer
857 supported by anodic aluminium oxide frame with nanochannels [192], and PDMS
858 (polydimethylsiloxane) micro-channels filled with Nafion [178].
859
860 nRED/μRED has been a rapidly developing area. Nevertheless, the existing studies are
861 generally based on very small membrane areas or even single pore. For several cases presented
862 in Table 3, low power density was obtained as a result of (1) the relative low pore density [177];
863 (2) relative large inter-membrane distance (e.g., 1.3 mm compared to commonly used 0.2 mm)
864 [192]; and (3) hindered diffusion transport of counter-ion due to increased number of co-ion in
865 nanopore networks with higher working area [187]. Future studies are needed to scale up such
866 technology and full cost-effectiveness of these novel membranes are yet to be validated.
867

868 **Table 3. Summary of reported power density of nRED/μRED in reviewed publications**

Salinity ratio	Nanochannels/nanopores type	Power density (W/m^2)	Reference	Year
1000	Track-etched conical nanopore	20-2600	[35]	2010
1000	Track-etched conical nanopore	8.3-14.3	[36]	2011
1000	Nanochannels formed by packed nanoparticles	2.820	[179]	2013
1000	Nanochannels formed by packed nanoparticles	0.020	[187]	2015
1000	Silica nanochannels	7.700	[175]	2010
1000	Paper based capillary	0.003	[119]	2015
2000	Nafion filled PDMS micro-channels	0.755	[178]	2016
100	Fumasep® dialysis microporous membrane	0.007	[182]	2011
50	Hybrid membrane of coating BCP on PET substrate with conical nanochannels	0.350	[177]	2015
50	Nanochannels in graphene oxide	0.770	[188]	2016
30	Polyelectrolytic coated anodic aluminium oxide	0.017	[192]	2016
10	Anodic alumina nanopores	0.007	[176]	2013
10	Silica coated on alumina substrate	0.001	[185]	2016

869

8. Conclusion

Salinity gradient power can be directly converted into electricity using RED technology. This review summarized the significant developments of RED in the last decade. Innovation in RED stack components and system design are crucial aspects to improve RED power output performance. To date, there have emerged several tailored IEMs of low resistance and high permselectivity to suit for RED applications. Furthermore, nanostructured IEMs with aligned nanochannels/nanopores showed power densities of several orders of magnitude higher over conventional IEMs. Nevertheless, scaling up of these membranes to large scale production remains as a key challenge. A proper spacer design shall provide uniform flow distribution, reduce shielding effect, and minimize pressure drop and fouling. The RED power density is significantly affected by the feed solution concentrations and temperatures. Using hypersaline solutions as HS are favored for providing high electromotive force, while there is an optimal concentration range of LS due to a compromise between electromotive force and internal resistance. Increasing attention has been given to hybrid processes, examples including converting thermal energy into electricity by closed-loop RED heat engine, microbial RED cell with boosted power performance, and low-energy (or even energy-free) desalination by integrating RED with desalination facilities. Despite the great achievements in the recent literature, full scale RED plants are not yet available. Additional pilot scale studies are needed to validate the feasibility of RED.

Acknowledgements

This work is supported by the Strategic Research Theme (Clean Energy) and the Seed Fund for Strategic Interdisciplinary Research Scheme, both funded by the University of Hong Kong.

References

[1] B.E. Logan, M. Elimelech, Membrane-based processes for sustainable power generation using water, Nature, 488 (2012) 313-319.

[2] K. Kwon, J. Han, B.H. Park, Y. Shin, D. Kim, Brine recovery using reverse electrodialysis in membrane-based desalination processes, Desalination, 362 (2015) 1-10.

[3] M. Tedesco, C. Scalici, D. Vaccari, A. Cipollina, A. Tamburini, G. Micale, Performance of the first reverse electrodialysis pilot plant for power production from saline waters and concentrated brines, Journal of Membrane Science, 500 (2016) 33-45.

[4] A. Daniilidis, D.A. Vermaas, R. Herber, K. Nijmeijer, Experimentally obtainable energy from mixing river water, seawater or brines with reverse electrodialysis, Renewable Energy, 64 (2014) 123-131.

[5] X. Luo, X. Cao, Y. Mo, K. Xiao, X. Zhang, P. Liang, X. Huang, Power generation by coupling reverse electrodialysis and ammonium bicarbonate: Implication for recovery of waste heat, Electrochemistry Communications, 19 (2012) 25-28.

[6] M.C. Hatzell, B.E. Logan, Evaluation of flow fields on bubble removal and system performance in an ammonium bicarbonate reverse electrodialysis stack, Journal of Membrane Science, 446 (2013) 449-455.

[7] K. Kwon, B.H. Park, D.H. Kim, D. Kim, Parametric study of reverse electrodialysis using ammonium bicarbonate solution for low-grade waste heat recovery, Energy Conversion and Management, 103 (2015) 104-110.

[8] R.S. Kingsbury, K. Chu, O. Coronell, Energy storage by reversible electrodialysis: The concentration battery, Journal of Membrane Science, 495 (2015) 502-516.

[9] W.J. van Egmond, M. Saakes, S. Porada, T. Meuwissen, C.J.N. Buisman, H.V.M. Hamelers, The concentration gradient flow battery as electricity storage system: Technology potential and energy dissipation, Journal of Power Sources, 325 (2016) 129-139.

[10] F. Helfer, C. Lemckert, Y.G. Anissimov, Osmotic power with Pressure Retarded Osmosis: Theory, performance and trends – A review, Journal of Membrane Science, 453 (2014) 337-358.

[11] N.Y. Yip, D. Brogioli, H.V. Hamelers, K. Nijmeijer, Salinity gradients for sustainable energy: Primer, progress, and prospects, Environmental Science & Technology, 50 (2016) 12072-12094.

[12] J.W. Post, J. Veerman, H.V.M. Hamelers, G.J.W. Euverink, S.J. Metz, K. Nymeijer, C.J.N. Buisman, Salinity-gradient power: Evaluation of pressure-retarded osmosis and reverse electrodialysis, Journal of Membrane Science, 288 (2007) 218-230.

[13] G.Z. Ramon, B.J. Feinberg, E.M.V. Hoek, Membrane-based production of salinity-gradient power, Energy & Environmental Science, 4 (2011) 4423.

[14] N.Y. Yip, M. Elimelech, Comparison of energy efficiency and power density in pressure retarded osmosis and reverse electrodialysis, Environmental Science & Technology, 48 (2014) 11002-11012.

[15] J.G. Hong, B. Zhang, S. Glabman, N. Uzal, X. Dou, H. Zhang, X. Wei, Y. Chen, Potential ion exchange membranes and system performance in reverse electrodialysis for power generation: A review, Journal of Membrane Science, 486 (2015) 71-88.

[16] J.G. Hong, J.J. Kim, Salinity Gradient Energy : Current Membrane Development and Challenges for Reverse Electrodialysis System, New & Renewable Energy, 12 (2016) 53.

[17] T. Xu, Ion exchange membranes: State of their development and perspective, Journal of Membrane Science, 263 (2005) 1-29.

[18] J.W. Post, H.V. Hamelers, C.J. Buisman, Energy recovery from controlled mixing salt and fresh water with a reverse electrodialysis system, Environmental Science & Technology, 42 (2008) 5785-5790.
[19] D.A. Vermaas, M. Saakes, K. Nijmeijer, Power generation using profiled membranes in reverse electrodialysis, Journal of Membrane Science, 385-386 (2011) 234-242.
[20] J. Gi Hong, Y. Chen, Evaluation of electrochemical properties and reverse electrodialysis performance for porous cation exchange membranes with sulfate-functionalized iron oxide, Journal of Membrane Science, 473 (2015) 210-217.
[21] D.H. Cho, K.H. Lee, Y.M. Kim, S.H. Park, W.H. Lee, S.M. Lee, Y.M. Lee, Effect of cationic groups in poly(arylene ether sulfone) membranes on reverse electrodialysis performance, Chemical communications, 53 (2017) 2323-2326.
[22] S.Y. Lee, Y.-J. Jeong, S.-R. Chae, K.-H. Yeon, Y. Lee, C.-S. Kim, N.-J. Jeong, J.-S. Park, Porous carbon-coated graphite electrodes for energy production from salinity gradient using reverse electrodialysis, Journal of Physics and Chemistry of Solids, 91 (2016) 34-40.
[23] Z. He, X. Gao, Y. Zhang, Y. Wang, J. Wang, Revised spacer design to improve hydrodynamics and anti-fouling behavior in reverse electrodialysis processes, Desalination and Water Treatment, 57 (2016) 28176-28186.
[24] R.E. Lacey, Energy by reverse electrodialysis, Ocean Engineering, 7 (1980) 1-47.
[25] J.N. Weinstein, F.B. Leitz, Electric power from differences in salinity: The dialytic battery, Science, 191 (1976) 557-559.
[26] X. Zhu, W. He, B.E. Logan, Influence of solution concentration and salt types on the performance of reverse electrodialysis cells, Journal of Membrane Science, 494 (2015) 154-160.
[27] M. Tedesco, E. Brauns, A. Cipollina, G. Micale, P. Modica, G. Russo, J. Helsen, Reverse electrodialysis with saline waters and concentrated brines: A laboratory investigation towards technology scale-up, Journal of Membrane Science, 492 (2015) 9-20.
[28] Y. Kim, B.E. Logan, Hydrogen production from inexhaustible supplies of fresh and salt water using microbial reverse-electrodialysis electrolysis cells, Proceedings of the National Academy of Sciences of the United States of America, 108 (2011) 16176-16181.
[29] W. Li, W.B. Krantz, E.R. Cornelissen, J.W. Post, A.R.D. Verliefde, C.Y. Tang, A novel hybrid process of reverse electrodialysis and reverse osmosis for low energy seawater desalination and brine management, Applied Energy, 104 (2013) 592-602.
[30] R.D. Cusick, Y. Kim, B.E. Logan, Energy capture from thermolytic solutions in microbial reverse-electrodialysis cells, Science, 335 (2012) 1474-1477.
[31] Y. Kim, B.E. Logan, Microbial reverse electrodialysis cells for synergistically enhanced power production, Environmental Science & Technology, 45 (2011) 5834-5839.
[32] Q. Chen, Y.-Y. Liu, C. Xue, Y.-L. Yang, W.-M. Zhang, Energy self-sufficient desalination stack as a potential fresh water supply on small islands, Desalination, 359 (2015) 52-58.
[33] F. Luo, Y. Wang, C. Jiang, B. Wu, H. Feng, T. Xu, A power free electrodialysis (PFED) for desalination, Desalination, 404 (2017) 138-146.
[34] Q. Wang, X. Gao, Y. Zhang, Z. He, Z. Ji, X. Wang, C. Gao, Hybrid RED/ED system: Simultaneous osmotic energy recovery and desalination of high-salinity wastewater, Desalination, 405 (2017) 59-67.
[35] W. Guo, L. Cao, J. Xia, F.-Q. Nie, W. Ma, J. Xue, Y. Song, D. Zhu, Y. Wang, L. Jiang, Energy harvesting with single-ion-selective nanopores: A concentration-gradient-driven nanofluidic power source, Advanced Functional Materials, 20 (2010) 1339-1344.
[36] L. Cao, W. Guo, W. Ma, L. Wang, F. Xia, S. Wang, Y. Wang, L. Jiang, D. Zhu, Towards understanding the nanofluidic reverse electrodialysis system: Well matched charge selectivity and ionic composition, Energy & Environmental Science, 4 (2011) 2259.

[37] D.A. Vermaas, D. Kunteng, M. Saakes, K. Nijmeijer, Fouling in reverse electrodialysis under natural conditions, Water research, 47 (2013) 1289-1298.
[38] M. Vaselbehagh, H. Karkhanechi, R. Takagi, H. Matsuyama, Biofouling phenomena on anion exchange membranes under the reverse electrodialysis process, Journal of Membrane Science, 530 (2017) 232-239.
[39] D.A. Vermaas, D. Kunteng, J. Veerman, M. Saakes, K. Nijmeijer, Periodic feedwater reversal and air sparging as antifouling strategies in reverse electrodialysis, Environmental Science & Technology, 48 (2014) 3065-3073.
[40] O. Scialdone, A. D'Angelo, E. De Lumè, A. Galia, Cathodic reduction of hexavalent chromium coupled with electricity generation achieved by reverse-electrodialysis processes using salinity gradients, Electrochimica Acta, 137 (2014) 258-265.
[41] O. Scialdone, A. D'Angelo, A. Galia, Energy generation and abatement of Acid Orange 7 in reverse electrodialysis cells using salinity gradients, Journal of Electroanalytical Chemistry, 738 (2015) 61-68.
[42] M. Tedesco, A. Cipollina, A. Tamburini, G. Micale, Towards 1kW power production in a reverse electrodialysis pilot plant with saline waters and concentrated brines, Journal of Membrane Science, 522 (2017) 226-236.
[43] R. Pattle, Production of electric power by mixing fresh and salt water in the hydroelectric pile, Nature, 174 (1954).
[44] J.C. Fair, Reverse electrodialysis in charged capillary membranes, The Journal of Chemical Physics, 54 (1971) 3307.
[45] F.E.K. BERT H. CLAMPITT, Energy recovery from saline water by means of electrochemical cells, Reports, (1976).
[46] G.L. Wick, Power from Salinity Gradients, Energy, 3 (1978) 95-100.
[47] R. Audinos, Reverse electrodialysis. Study of the electric energy obtained by mixing two solutions of different salinity, Journal of Power Sources, 10 (1983) 203-217.
[48] H. Ohya, Dialytic battery convertible free energy of mixing of sea water and river water, in: Organized by Korean Inst of Chemical Engineers, 1983, pp. 451-456.
[49] S. Ratkje, T. Holt, L. Fiksdal, Effect of biofilm formation on salinity power plant output on a laboratory scale, in: AIChE Symp. Ser, 1986, pp. 39-44.
[50] J. Jagur-Grodzinski, R. Kramer, Novel process for direct conversion of free energy of mixing into electric power, Industrial & Engineering Chemistry Process Design and Development, 25 (1986) 443-449.
[51] E. Brauns, Towards a worldwide sustainable and simultaneous large-scale production of renewable energy and potable water through salinity gradient power by combining reversed electrodialysis and solar power?, Desalination, 219 (2008) 312-323.
[52] P. Długołęcki, J. Dąbrowska, K. Nijmeijer, M. Wessling, Ion conductive spacers for increased power generation in reverse electrodialysis, Journal of Membrane Science, 347 (2010) 101-107.
[53] A. Achilli, A.E. Childress, Pressure retarded osmosis: From the vision of Sidney Loeb to the first prototype installation — Review, Desalination, 261 (2010) 205-211.
[54] P. Dlugolecki, K. Nymeijer, S. Metz, M. Wessling, Current status of ion exchange membranes for power generation from salinity gradients, Journal of Membrane Science, 319 (2008) 214-222.
[55] J. Veerman, R.M. de Jong, M. Saakes, S.J. Metz, G.J. Harmsen, Reverse electrodialysis: Comparison of six commercial membrane pairs on the thermodynamic efficiency and power density, Journal of Membrane Science, 343 (2009) 7-15.
[56] J. Veerman, J.W. Post, M. Saakes, S.J. Metz, G.J. Harmsen, Reducing power losses caused by ionic shortcut currents in reverse electrodialysis stacks by a validated model, Journal of Membrane Science, 310 (2008) 418-430.

[57] P. Dlugolecki, A. Gambier, K. Nijmeijer, M. Wessling, Practical potential of reverse electrodialysis as process for sustainable energy generation, Environmental Science & Technology, 43 (2009) 6888-6894.
[58] M. Turek, B. Bandura, Renewable energy by reverse electrodialysis, Desalination, 205 (2007) 67-74.
[59] E. Brauns, Salinity gradient power by reverse electrodialysis: Effect of model parameters on electrical power output, Desalination, 237 (2009) 378-391.
[60] J. Veerman, M. Saakes, S.J. Metz, G.J. Harmsen, Reverse electrodialysis: Performance of a stack with 50 cells on the mixing of sea and river water, Journal of Membrane Science, 327 (2009) 136-144.
[61] M. Turek, B. Bandura, P. Dydo, Power production from coal-mine brine utilizing reversed electrodialysis, Desalination, 221 (2008) 462-466.
[62] E. Guler, Y. Zhang, M. Saakes, K. Nijmeijer, Tailor-made anion-exchange membranes for salinity gradient power generation using reverse electrodialysis, ChemSusChem, 5 (2012) 2262-2270.
[63] J.G. Hong, Y. Chen, Nanocomposite reverse electrodialysis (RED) ion-exchange membranes for salinity gradient power generation, Journal of Membrane Science, 460 (2014) 139-147.
[64] S. Lee, M.-S. Shin, J.-S. Park, Anion-conducting pore-filling membranes with optimization of transport number and resistance for reverse electrodialysis, Chemistry Letters, 43 (2014) 621-623.
[65] J.Y. Lee, J.H. Kim, J.H. Lee, S. Kim, S.H. Moon, Morphologically aligned cation-exchange membranes by a pulsed electric field for reverse electrodialysis, Environmental Science & Technology, (2015).
[66] H. Kim, M.S. Lee, S. Lee, Y.W. Choi, N. Jeong, C. Kim, High power density of reverse electrodialysis with pore-filling ion exchange membranes and high-open-area spacer, Journal of Materials Chemistry A, (2015).
[67] E. Güler, R. Elizen, M. Saakes, K. Nijmeijer, Micro-structured membranes for electricity generation by reverse electrodialysis, Journal of Membrane Science, 458 (2014) 136-148.
[68] B. Zhang, H. Gao, Y. Chen, Enhanced ionic conductivity and power generation using ion-exchange resin beads in a reverse-electrodialysis stack, Environmental Science & Technology, 49 (2015) 14717-14724.
[69] W.J. van Egmond, U.K. Starke, M. Saakes, C.J.N. Buisman, H.V.M. Hamelers, Energy efficiency of a concentration gradient flow battery at elevated temperatures, Journal of Power Sources, 340 (2017) 71-79.
[70] O. Scialdone, A. D'Angelo, E. De Lume, A. Galia, Utilization of reverse electrodialysis processes for the abatement of pollutants in water, 10th Esee: European Symposium on Electrochemical Engineering, 41 (2014) 139-144.
[71] R. B.V., Dutch king officially opens Blue Energy pilot installation on the Afsluitdijk, http://www.redstack.nl/en/news/83/dutch-king-officially-opens-blue-energy-pilot-installation-on-the-afsluitdijk, November, 2014.
[72] S. Pawlowski, C.F. Galinha, J.G. Crespo, S. Velizarov, Prediction of reverse electrodialysis performance by inclusion of 2D fluorescence spectroscopy data into multivariate statistical models, Separation and Purification Technology, 150 (2015) 159-169.
[73] C. Jiang, Y. Wang, T. Xu, An excellent method to produce morpholine by bipolar membrane electrodialysis, Separation and Purification Technology, 115 (2013) 100-106.
[74] H. Strathmann, Electrodialysis, a mature technology with a multitude of new applications, Desalination, 264 (2010) 268-288.

[75] T. Cath, A. Childress, M. Elimelech, Forward osmosis: Principles, applications, and recent developments, Journal of Membrane Science, 281 (2006) 70-87.
[76] Y. Xu, X. Peng, C.Y. Tang, Q.S. Fu, S. Nie, Effect of draw solution concentration and operating conditions on forward osmosis and pressure retarded osmosis performance in a spiral wound module, Journal of Membrane Science, 348 (2010) 298-309.
[77] S. Zhao, L. Zou, C.Y. Tang, D. Mulcahy, Recent developments in forward osmosis: Opportunities and challenges, Journal of Membrane Science, 396 (2012) 1-21.
[78] T. Yun, Y.-J. Kim, S. Lee, S. Hong, G.I. Kim, Flux behavior and membrane fouling in pressure-assisted forward osmosis, Desalination and Water Treatment, 52 (2013) 564-569.
[79] J. Duan, E. Litwiller, I. Pinnau, Solution-diffusion with defects model for pressure-assisted forward osmosis, Journal of Membrane Science, 470 (2014) 323-333.
[80] K.A. Stancheva, Applications of dialysis, Oxidation Communications, 31 (2008) 758-775.
[81] P. Wang, G. Zhang, Y. Wu, Diffusion dialysis for separating acidic HCl/glyphosate liquor, Separation and Purification Technology, 141 (2015) 387-393.
[82] X. Lin, E. Shamsaei, B. Kong, J.Z. Liu, Y. Hu, T. Xu, H. Wang, Porous diffusion dialysis membranes for rapid acid recovery, Journal of Membrane Science, 502 (2016) 76-83.
[83] X. Tongwen, Y. Weihua, Industrial recovery of mixed acid (HF + HNO_3) from the titanium spent leaching solutions by diffusion dialysis with a new series of anion exchange membranes, Journal of Membrane Science, 220 (2003) 89-95.
[84] J. Xu, S. Lu, D. Fu, Recovery of hydrochloric acid from the waste acid solution by diffusion dialysis, Journal of hazardous materials, 165 (2009) 832-837.
[85] J. Luo, C. Wu, T. Xu, Y. Wu, Diffusion dialysis-concept, principle and applications, Journal of Membrane Science, 366 (2011) 1-16.
[86] X. Zhang, X. Wang, C. Li, H. Feng, Q. Li, Y. Wang, G. Wang, T. Xu, A preliminary study on electrically assisted diffusion dialysis, Separation and Purification Technology, 122 (2014) 331-340.
[87] N.Y. Yip, M. Elimelech, Thermodynamic and energy efficiency analysis of power generation from natural salinity gradients by pressure retarded osmosis, Environmental Science & Technology, 46 (2012) 5230-5239.
[88] D.A. Vermaas, J. Veerman, N.Y. Yip, M. Elimelech, M. Saakes, K. Nijmeijer, High efficiency in energy generation from salinity gradients with reverse electrodialysis, ACS Sustainable Chemistry & Engineering, 1 (2013) 1295-1302.
[89] N.Y. Yip, D.A. Vermaas, K. Nijmeijer, M. Elimelech, Thermodynamic, energy efficiency, and power density analysis of reverse electrodialysis power generation with natural salinity gradients, Environmental Science & Technology, (2014).
[90] D.A. Vermaas, M. Saakes, K. Nijmeijer, Doubled power density from salinity gradients at reduced intermembrane distance, Environmental Science & Technology, 45 (2011) 7089-7095.
[91] M.Y. Kariduraganavar, R.K. Nagarale, A.A. Kittur, S.S. Kulkarni, Ion-exchange membranes: preparative methods for electrodialysis and fuel cell applications, Desalination, 197 (2006) 225-246.
[92] R.K. Nagarale, G.S. Gohil, V.K. Shahi, Recent developments on ion-exchange membranes and electro-membrane processes, Advances in Colloid and Interface Science, 119 (2006) 97-130.
[93] J. Ran, L. Wu, Y. He, Z. Yang, Y. Wang, C. Jiang, L. Ge, E. Bakangura, T. Xu, Ion exchange membranes: New developments and applications, Journal of Membrane Science, 522 (2017) 267-291.
[94] H. Zhang, D. Jiang, B. Zhang, J.G. Hong, Y. Chen, A novel hybrid poly (vinyl alcohol) (PVA)/poly (2,6-dimethyl-1,4-phenylene oxide) (PPO) membranes for reverse electrodialysis power system, Electrochimica Acta, (2017).

[95] G.M. Geise, M.A. Hickner, B.E. Logan, Ionic resistance and permselectivity tradeoffs in anion exchange membranes, ACS applied materials & interfaces, 5 (2013) 10294-10301.
[96] E. Güler, R. Elizen, D.A. Vermaas, M. Saakes, K. Nijmeijer, Performance-determining membrane properties in reverse electrodialysis, Journal of Membrane Science, 446 (2013) 266-276.
[97] M.C. Wijers, M. Jin, M. Wessling, H. Strathmann, Supported liquid membranes modification with sulphonated poly(ether ether ketone). Permeability, selectivity and stability, Journal of Membrane Science, 147 (1998) 117-130.
[98] H. Strathmann, A. Grabowski, G. Eigenberger, Ion-Exchange Membranes in the Chemical Process Industry, Industrial & Engineering Chemistry Research, 52 (2013) 10364-10379.
[99] A.H. Galama, D.A. Vermaas, J. Veerman, M. Saakes, H.H.M. Rijnaarts, J.W. Post, K. Nijmeijer, Membrane resistance: The effect of salinity gradients over a cation exchange membrane, Journal of Membrane Science, 467 (2014) 279-291.
[100] M.L. Disabb-Miller, Z.D. Johnson, M.A. Hickner, Ion motion in snion and proton-conducting triblock copolymers, Macromolecules, 46 (2013) 949-956.
[101] G.M. Geise, L.P. Falcon, B.D. Freeman, D.R. Paul, Sodium chloride sorption in sulfonated polymers for membrane applications, Journal of Membrane Science, 423-424 (2012) 195-208.
[102] F.G. Helfferich, Ion Exchange, McGraw-Hill, 1962.
[103] T. Sata, Preparation of ion exchange membranes, (2007) 35-88.
[104] H. Strathmann, Ion-exchange Membrane Separation Processes (first ed.)
2004.
[105] P. Długołęcki, P. Ogonowski, S.J. Metz, M. Saakes, K. Nijmeijer, M. Wessling, On the resistances of membrane, diffusion boundary layer and double layer in ion exchange membrane transport, Journal of Membrane Science, 349 (2010) 369-379.
[106] G.M. Geise, A.J. Curtis, M.C. Hatzell, M.A. Hickner, B.E. Logan, Salt concentration differences alter membrane resistance in reverse electrodialysis stacks, Environmental Science & Technology Letters, 1 (2014) 36-39.
[107] J. Gi Hong, S. Glabman, Y. Chen, Effect of inorganic filler size on electrochemical performance of nanocomposite cation exchange membranes for salinity gradient power generation, Journal of Membrane Science, 482 (2015) 33-41.
[108] X. Tong, B. Zhang, Y. Chen, Fouling resistant nanocomposite cation exchange membrane with enhanced power generation for reverse electrodialysis, Journal of Membrane Science, 516 (2016) 162-171.
[109] E.Y. Safronova, D.V. Golubenko, N.V. Shevlyakova, M.G. D'yakova, V.A. Tverskoi, L. Dammak, D. Grande, A.B. Yaroslavtsev, New cation-exchange membranes based on cross-linked sulfonated polystyrene and polyethylene for power generation systems, Journal of Membrane Science, 515 (2016) 196-203.
[110] J. Liu, G.M. Geise, X. Luo, H. Hou, F. Zhang, Y. Feng, M.A. Hickner, B.E. Logan, Patterned ion exchange membranes for improved power production in microbial reverse-electrodialysis cells, Journal of Power Sources, 271 (2014) 437-443.
[111] F. Suda, T. Matsuo, D. Ushioda, Transient changes in the power output from the concentration difference cell (dialytic battery) between seawater and river water, Energy, 32 (2007) 165-173.
[112] A.H. Avci, P. Sarkar, R.A. Tufa, D. Messana, P. Argurio, E. Fontananova, G. Di Profio, E. Curcio, Effect of Mg^{2+} ions on energy generation by reverse electrodialysis, Journal of Membrane Science, 520 (2016) 499-506.
[113] M. Bevacqua, A. Carubia, A. Cipollina, A. Tamburini, M. Tedesco, G. Micale, Performance of a RED system with ammonium hydrogen carbonate solutions, Desalination and Water Treatment, (2016) 1-12.

[114] E. Fontananova, D. Messana, R.A. Tufa, I. Nicotera, V. Kosma, E. Curcio, W. van Baak, E. Drioli, G. Di Profio, Effect of solution concentration and composition on the electrochemical properties of ion exchange membranes for energy conversion, Journal of Power Sources, 340 (2017) 282-293.
[115] Ramato A. Tufa, E. Curcio, E. Brauns, W. van Baak, E. Fontananova, G. Di Profio, Membrane distillation and reverse electrodialysis for near-zero liquid discharge and low energy seawater desalination, Journal of Membrane Science, 496 (2015) 325-333.
[116] R.A. Tufa, E. Curcio, W. van Baak, J. Veerman, S. Grasman, E. Fontananova, G. Di Profio, Potential of brackish water and brine for energy generation by salinity gradient power-reverse electrodialysis (SGP-RE), RSC Adv., 4 (2014) 42617-42623.
[117] D.A. Vermaas, J. Veerman, M. Saakes, K. Nijmeijer, Influence of multivalent ions on renewable energy generation in reverse electrodialysis, Energy & Environmental Science, 7 (2014) 1434.
[118] J. Moreno, E. Slouwerhof, D.A. Vermaas, M. Saakes, K. Nijmeijer, The breathing cell: cyclic intermembrane distance variation in reverse electrodialysis, Environmental Science & Technology, (2016).
[119] H.-K. Chang, E. Choi, J. Park, Paper-based energy harvesting from salinity gradients, Lab Chip, 16 (2016) 700-708.
[120] X. Zhu, W. He, B.E. Logan, Reducing pumping energy by using different flow rates of high and low concentration solutions in reverse electrodialysis cells, Journal of Membrane Science, 486 (2015) 215-221.
[121] D.A. Vermaas, M. Saakes, K. Nijmeijer, Enhanced mixing in the diffusive boundary layer for energy generation in reverse electrodialysis, Journal of Membrane Science, 453 (2014) 312-319.
[122] H. Kim, M.S. Lee, S. Lee, Y.W. Choi, N. Jeong, C. Kim, High power density of reverse electrodialysis with pore-filling ion exchange membranes and high-open-area spacer, J. Mater. Chem. A, (2015).
[123] B. Zhang, J.G. Hong, S. Xie, S. Xia, Y. Chen, An integrative modeling and experimental study on the ionic resistance of ion-exchange membranes, Journal of Membrane Science, 524 (2017) 362-369.
[124] K. Kwon, B.-H. Park, D.H. Kim, D. Kim, Comparison of spacer-less and spacer-filled reverse electrodialysis, Journal of Renewable and Sustainable Energy, 9 (2017) 044502.
[125] J. Veerman, M. Saakes, S.J. Metz, G.J. Harmsen, Reverse electrodialysis: A validated process model for design and optimization, Chemical Engineering Journal, 166 (2011) 256-268.
[126] L. Gurreri, A. Tamburini, A. Cipollina, G. Micale, CFD analysis of the fluid flow behavior in a reverse electrodialysis stack, Desalination and Water Treatment, 48 (2012) 390-403.
[127] L. Gurreri, A. Tamburini, A. Cipollina, G. Micale, M. Ciofalo, CFD simulation of mass transfer phenomena in spacer filled channels for reverse electrodialysis applications, Chem Engineer Trans, 32 (2013) 1879-1884.
[128] D.A. Vermaas, E. Guler, M. Saakes, K. Nijmeijer, Theoretical power density from salinity gradients using reverse electrodialysis, Energy Procedia, 20 (2012) 170-184.
[129] S. Pawlowski, V. Geraldes, J.G. Crespo, S. Velizarov, Computational fluid dynamics (CFD) assisted analysis of profiled membranes performance in reverse electrodialysis, Journal of Membrane Science, 502 (2016) 179-190.
[130] S. Pawlowski, T. Rijnaarts, M. Saakes, K. Nijmeijer, J.G. Crespo, S. Velizarov, Improved fluid mixing and power density in reverse electrodialysis stacks with chevron-profiled membranes, Journal of Membrane Science, 531 (2017) 111-121.

[131] A.M. Lopez, H. Dunsworth, J.A. Hestekin, Reduction of the shadow spacer effect using reverse electrodeionization and its applications in water recycling for hydraulic fracturing operations, Separation and Purification Technology, 162 (2016) 84-90.
[132] S. Pawlowski, P. Sistat, J.G. Crespo, S. Velizarov, Mass transfer in reverse electrodialysis: Flow entrance effects and diffusion boundary layer thickness, Journal of Membrane Science, 471 (2014) 72-83.
[133] S. Pawlowski, J.G. Crespo, S. Velizarov, Pressure drop in reverse electrodialysis: Experimental and modeling studies for stacks with variable number of cell pairs, Journal of Membrane Science, 462 (2014) 96-111.
[134] J. Veerman, M. Saakes, S.J. Metz, G.J. Harmsen, Electrical power from sea and river water by reverse electrodialysis: a first step from the laboratory to a real power plant, Environmental Science & Technology, 44 (2010) 9207-9212.
[135] J. Veerman, M. Saakes, S.J. Metz, G.J. Harmsen, Reverse electrodialysis: evaluation of suitable electrode systems, Journal of Applied Electrochemistry, 40 (2010) 1461-1474.
[136] O. Scialdone, C. Guarisco, S. Grispo, A.D. Angelo, A. Galia, Investigation of electrode material – Redox couple systems for reverse electrodialysis processes. Part I: Iron redox couples, Journal of Electroanalytical Chemistry, 681 (2012) 66-75.
[137] R. Audinos, Electric-power produced from 2 solutions of unequal salinity by reverse electrodialysis, Indian Journal of Chemistry Section A: Inorganic Bio-inorganic Physical Theoretical & Analytical Chemistry, 31 (1992) 348-354.
[138] O.S. Burheim, F. Seland, J.G. Pharoah, S. Kjelstrup, Improved electrode systems for reverse electro-dialysis and electro-dialysis, Desalination, 285 (2012) 147-152.
[139] J.Y. Nam, R.D. Cusick, Y. Kim, B.E. Logan, Hydrogen generation in microbial reverse-electrodialysis electrolysis cells using a heat-regenerated salt solution, Environmental Science & Technology, 46 (2012) 5240-5246.
[140] M. Tedesco, A. Cipollina, A. Tamburini, W. van Baak, G. Micale, Modelling the reverse electrodialysis process with seawater and concentrated brines, Desalination and Water Treatment, 49 (2012) 404-424.
[141] K. Kwon, S.J. Lee, L. Li, C. Han, D. Kim, Energy harvesting system using reverse electrodialysis with nanoporous polycarbonate track-etch membranes, International Journal of Energy Research, 38 (2014) 530-537.
[142] M. Tedesco, A. Cipollina, A. Tamburini, G. Micale, J. Helsen, M. Papapetrou, REAPower: Use of desalination brine for power production through reverse electrodialysis, Desalination and Water Treatment, 53 (2014) 3161-3169.
[143] A. Emdadi, P. Gikas, M. Farazaki, Y. Emami, Salinity gradient energy potential at the hyper saline Urmia Lake – ZarrinehRud River system in Iran, Renewable Energy, 86 (2016) 154-162.
[144] Y. Mei, C.Y. Tang, Co-locating reverse electrodialysis with reverse osmosis desalination: Synergies and implications, Journal of Membrane Science, (2017).
[145] L. Gurreri, A. Tamburini, A. Cipollina, G. Micale, M. Ciofalo, CFD prediction of concentration polarization phenomena in spacer-filled channels for reverse electrodialysis, Journal of Membrane Science, 468 (2014) 133-148.
[146] J.G. Hong, W. Zhang, J. Luo, Y. Chen, Modeling of power generation from the mixing of simulated saline and freshwater with a reverse electrodialysis system: The effect of monovalent and multivalent ions, Applied Energy, 110 (2013) 244-251.
[147] J.W. Post, H.V.M. Hamelers, C.J.N. Buisman, Influence of multivalent ions on power production from mixing salt and fresh water with a reverse electrodialysis system, Journal of Membrane Science, 330 (2009) 65-72.
[148] E. Güler, W. van Baak, M. Saakes, K. Nijmeijer, Monovalent-ion-selective membranes for reverse electrodialysis, Journal of Membrane Science, 455 (2014) 254-270.

[149] A.M. Weiner, R.K. McGovern, J.H.L. V, A new reverse electrodialysis design strategy which significantly reduces the levelized cost of electricity, Journal of Membrane Science, (2015).
[150] E. Brauns, An alternative hybrid concept combining seawater desalination, solar energy and reverse electrodialysis for a sustainable production of sweet water and electrical energy, Desalination and Water Treatment, 13 (2010) 53-62.
[151] R.S. Kingsbury, F. Liu, S. Zhu, C. Boggs, M.D. Armstrong, D.F. Call, O. Coronell, Impact of natural organic matter and inorganic solutes on energy recovery from five real salinity gradients using reverse electrodialysis, Journal of Membrane Science, 541 (2017) 621-632.
[152] J. Moreno, N. de Hart, M. Saakes, K. Nijmeijer, CO_2 saturated water as two-phase flow for fouling control in reverse electrodialysis, Water Research, 125 (2017) 23-31.
[153] J. Nikkola, X. Liu, Y. Li, M. Raulio, H.L. Alakomi, J. Wei, C.Y. Tang, Surface modification of thin film composite RO membrane for enhanced anti-biofouling performance, Journal of Membrane Science, 444 (2013) 192-200.
[154] E.S. Kim, Q. Yu, B. Deng, Plasma surface modification of nanofiltration (NF) thin-film composite (TFC) membranes to improve anti organic fouling, Applied Surface Science, 257 (2011) 9863-9871.
[155] G.M. Geise, M.A. Hickner, B.E. Logan, Ammonium Bicarbonate Transport in Anion Exchange Membranes for Salinity Gradient Energy, ACS Macro Letters, 2 (2013) 814-817.
[156] Y.A. Jande, W.S. Kim, Integrating reverse electrodialysis with constant current operating capacitive deionization, Journal of Environmental Management, 146 (2014) 463-469.
[157] W. Huang, W.S. Walker, Y. Kim, Junction potentials in thermolytic reverse electrodialysis, Desalination, 369 (2015) 149-155.
[158] D.H. Kim, B.H. Park, K. Kwon, L. Li, D. Kim, Modeling of power generation with thermolytic reverse electrodialysis for low-grade waste heat recovery, Applied Energy, 189 (2017) 201-210.
[159] X. Luo, F. Zhang, J. Liu, X. Zhang, X. Huang, B.E. Logan, Methane production in microbial reverse-electrodialysis methanogenesis cells (MRMCs) using thermolytic solutions, Environmental Science & Technology, 48 (2014) 8911-8918.
[160] X. Luo, J.Y. Nam, F. Zhang, X. Zhang, P. Liang, X. Huang, B.E. Logan, Optimization of membrane stack configuration for efficient hydrogen production in microbial reverse-electrodialysis electrolysis cells coupled with thermolytic solutions, Bioresource Technology, 140 (2013) 399-405.
[161] R.D. Cusick, M. Hatzell, F. Zhang, B.E. Logan, Minimal RED cell pairs markedly improve electrode kinetics and power production in microbial reverse electrodialysis cells, Environmental Science & Technology, 47 (2013) 14518-14524.
[162] V.J. Watson, M. Hatzell, B.E. Logan, Hydrogen production from continuous flow, microbial reverse-electrodialysis electrolysis cells treating fermentation wastewater, Bioresource Technology, (2015).
[163] S. Hidayat, Y.-H. Song, J.-Y. Park, A comparison of mono- and multi-valent ions as stack feed solutions in microbial reverse-electrodialysis electrolysis cells and their effects on hydrogen generation, International Biodeterioration & Biodegradation, 113 (2016) 28-33.
[164] Y.H. Song, S. Hidayat, H.K. Kim, J.Y. Park, Hydrogen production in microbial reverse-electrodialysis electrolysis cells using a substrate without buffer solution, Bioresource Technology, 210 (2016) 56-60.
[165] X. Zhu, M.C. Hatzell, R.D. Cusick, B.E. Logan, Microbial reverse-electrodialysis chemical-production cell for acid and alkali production, Electrochemistry Communications, 31 (2013) 52-55.

[166] X. Li, I. Angelidaki, Y. Zhang, Salinity-gradient energy driven microbial electrosynthesis of hydrogen peroxide, Journal of Power Sources, 341 (2017) 357-365.
[167] X. Li, X. Jin, N. Zhao, I. Angelidaki, Y. Zhang, Novel bio-electro-Fenton technology for azo dye wastewater treatment using microbial reverse-electrodialysis electrolysis cell, Bioresource Technology, 228 (2017) 322-329.
[168] X. Zhu, M.C. Hatzell, B.E. Logan, Microbial Reverse-Electrodialysis Electrolysis and Chemical-Production Cell for H Production and CO Sequestration, Environmental Science & Technology Letters, 1 (2014) 231-235.
[169] A. D'Angelo, A. Galia, O. Scialdone, Cathodic abatement of Cr(VI) in water by microbial reverse-electrodialysis cells, Journal of Electroanalytical Chemistry, 748 (2015) 40-46.
[170] M.C. Hatzell, I. Ivanov, R.D. Cusick, X. Zhu, B.E. Logan, Comparison of hydrogen production and electrical power generation for energy capture in closed-loop ammonium bicarbonate reverse electrodialysis systems, Physical Chemistry Chemical Physics : PCCP, 16 (2014) 1632-1638.
[171] Y.A.C. Jande, W.-S. Kim, Simultaneous Production of freshwater and energy from saline water using hybrid capacitive mixing reverse electrodialysis, (2014).
[172] R.A. Tufa, E. Rugiero, D. Chanda, J. Hnàt, W. van Baak, J. Veerman, E. Fontananova, G. Di Profio, E. Drioli, K. Bouzek, E. Curcio, Salinity gradient power-reverse electrodialysis and alkaline polymer electrolyte water electrolysis for hydrogen production, Journal of Membrane Science, 514 (2016) 155-164.
[173] E. Farrell, M.I. Hassan, R.A. Tufa, A. Tuomiranta, A.H. Avci, A. Politano, E. Curcio, H.A. Arafat, Reverse electrodialysis powered greenhouse concept for water- and energy-self-sufficient agriculture, Applied Energy, 187 (2017) 390-409.
[174] X. Zhu, T. Kim, M. Rahimi, C.A. Gorski, B.E. Logan, Integrating reverse-electrodialysis stacks with flow batteries for improved energy recovery from salinity gradients and energy storage, ChemSusChem, 10 (2017) 797-803.
[175] D.-K. Kim, C. Duan, Y.-F. Chen, A. Majumdar, Power generation from concentration gradient by reverse electrodialysis in ion-selective nanochannels, Microfluidics and Nanofluidics, 9 (2010) 1215-1224.
[176] J. Kim, S.J. Kim, D.-K. Kim, Energy harvesting from salinity gradient by reverse electrodialysis with anodic alumina nanopores, Energy, 51 (2013) 413-421.
[177] Z. Zhang, X.Y. Kong, K. Xiao, Q. Liu, G. Xie, P. Li, J. Ma, Y. Tian, L. Wen, L. Jiang, Engineered asymmetric heterogeneous membrane: A concentration-gradient-driven energy harvesting device, Journal of the American Chemical Society, 137 (2015) 14765-14772.
[178] T.-C. Tsai, C.-W. Liu, R.-J. Yang, Power generation by reverse electrodialysis in a microfluidic device with a Nafion ion-selective membrane, Micromachines, 7 (2016) 205.
[179] W. Ouyang, W. Wang, H. Zhang, W. Wu, Z. Li, Nanofluidic crystal: a facile, high-efficiency and high-power-density scaling up scheme for energy harvesting based on nanofluidic reverse electrodialysis, Nanotechnology, 24 (2013) 345401.
[180] D.J. Rankin, D.M. Huang, The effect of hydrodynamic slip on membrane-based salinity-gradient-driven energy harvesting, Langmuir : the ACS journal of surfaces and colloids, 32 (2016) 3420-3432.
[181] S. Tseng, Y.-M. Li, C.-Y. Lin, J.-P. Hsu, Salinity gradient power: Optimization of nanopore size, Electrochimica Acta, 219 (2016) 790-797.
[182] R. Banan Sadeghian, O. Pantchenko, D. Tate, A. Shakouri, Miniaturized concentration cells for small-scale energy harvesting based on reverse electrodialysis, Applied Physics Letters, 99 (2011) 173702.
[183] H.-C. Yeh, C.-C. Chang, R.-J. Yang, Reverse electrodialysis in conical-shaped nanopores: salinity gradient-driven power generation, RSC Adv., 4 (2014) 2705-2714.

[184] D.-K. Kim, Numerical study of power generation by reverse electrodialysis in ion-selective nanochannels, Journal of Mechanical Science and Technology, 25 (2011) 5-10.
[185] S. Lee, H. Kim, D.-K. Kim, Power generation from concentration gradient by reverse electrodialysis in dense silica membranes for microfluidic and nanofluidic systems, Energies, 9 (2016) 49.
[186] E. Choi, K. Kwon, D. Kim, J. Park, Nanofluidic reverse electrodialysis platform using controlled assembly of nanoparticles for high power energy generation, 2014 Ieee 27th International Conference on Micro Electro Mechanical Systems (Mems), (2014) 421-424.
[187] E. Choi, K. Kwon, D. Kim, J. Park, Tunable reverse electrodialysis microplatform with geometrically controlled self-assembled nanoparticle network, Lab Chip, 15 (2015) 168-178.
[188] J. Ji, Q. Kang, Y. Zhou, Y. Feng, X. Chen, J. Yuan, W. Guo, Y. Wei, L. Jiang, Osmotic power generation with positively and negatively charged 2D nanofluidic membrane pairs, Advanced Functional Materials, (2016).
[189] B. Kang, J. Yoo, H.J. Kim, D.-K. Kim, Slip-enhanced reverse electrodialytic power generation in ion-selective nanochannels, Journal of Thermal Science, 22 (2013) 36-41.
[190] S. Tseng, Y.-M. Li, C.-Y. Lin, J.-P. Hsu, Salinity gradient power: Influences of temperature and nanopore size, Nanoscale, 8 (2016) 2350-2357.
[191] C. Wang, E. Choi, G.T. Jang, J. Park, Effect of ion current rectification on energy harvesting by reverse electrodialysis, Proc Ieee Micr Elect, (2016) 1240-1243.
[192] S.H. Kwak, S.R. Kwon, S. Baek, S.M. Lim, Y.C. Joo, T.D. Chung, Densely charged polyelectrolyte-stuffed nanochannel arrays for power generation from salinity gradient, Scientific Reports, 6 (2016) 26416.